INVESTIGATION OF THE FEASIBILITY OF THE ELECTRON BEAM-EXCITED, HIGH-PRESSURE RECOMBINATION LASER

TEXAS UNIVERSITY

PREPARED FOR
OFFICE OF NAVAL RESEARCH
ADVANCED RESEARCH PROJECTS AGENCY

OCTOBER 1973

Security Classification

AD 769 833

DOCUMENT CONTROL DATA - R & D

(Security classification of title, body of abstract and indexing annotation must be entered when the overall report is classified)

1. ORIGINATING ACTIVITY *(Corporate author)*
The University of Texas at Dallas
P. O. Box 30365
Dallas, Texas 75230

2a. REPORT SECURITY CLASSIFICATION
UNCLASSIFIED

2b. GROUP

3. REPORT TITLE
INVESTIGATION OF THE FEASIBILITY OF THE ELECTRON BEAM-EXCITED, HIGH-PRESSURE RECOMBINATION LASER

4. DESCRIPTIVE NOTES *(Type of report and inclusive dates)*
Third Semi-Annual Technical Report (period covered by this report 4/1/73-9/1/73)

5. AUTHOR(S) *(First name, middle initial, last name)*
Carl B. Collins
Austin J. Cunningham
Brian W. Johnson

6. REPORT DATE	7a. TOTAL NO. OF PAGES	7b. NO. OF REFS
21, October 1973	115	17

8a. CONTRACT OR GRANT NO.	9a. ORIGINATOR'S REPORT NUMBER(S)
N00014-67-A-0310-0007	UTDP A002-3
b. PROJECT NO. ARPA Order No. 1807	
c. Program Code 2E90	9b. OTHER REPORT NO(S) *(Any other numbers that may be assigned this report)*
d.	

10. DISTRIBUTION STATEMENT
Distribution of this document is unlimited.

11. SUPPLEMENTARY NOTES	12. SPONSORING MILITARY ACTIVITY
	Office of Naval Research

13. ABSTRACT

This report describes research applied toward the determination of the feasibility of developing a recombining, electron beam-excited plasma into a pulsed laser of exceptionally high peak power.

19

DD FORM 1 NOV 65 1473

Security Classification

14. KEY WORDS	LINK A		LINK B		LINK C	
	ROLE	WT	ROLE	WT	ROLE	WT
Recombination Laser						
Laser						

Third Semi-Annual Technical Report

Item A002

Period Ending 1, September, 1973

Short Title: RECOMBINATION LASER

ARPA Order Number 1807

Program Code Number 2E90

Contract Number N00014-67-A0310-0007

Principal Investigator: C. B. Collins
The University of Texas at Dallas
P. O. Box 30365
Dallas, Texas 75230
(214) 231-1471

Contractor: The Board of Regents of
The University of Texas System

Scientific Officer: Director
Physics Programs,
Physical Sciences Division
Office of Naval Research
Department of the Navy
800 N. Quincy Street
Arlington, Virginia 22217

Effective Date of Contract : 21 March 1972

Expiration Date of Contract : 31 December 1973

Amount of Contract	:	$ 99,990.00
Amount of Modification #1	:	91,400.00
Total Amount	:	$191,390.00

Sponsored by

Advanced Research Projects Agency

ARPA Order No. 1807

Form Approved Budget Bureau No. 22-R0293

CONTENTS

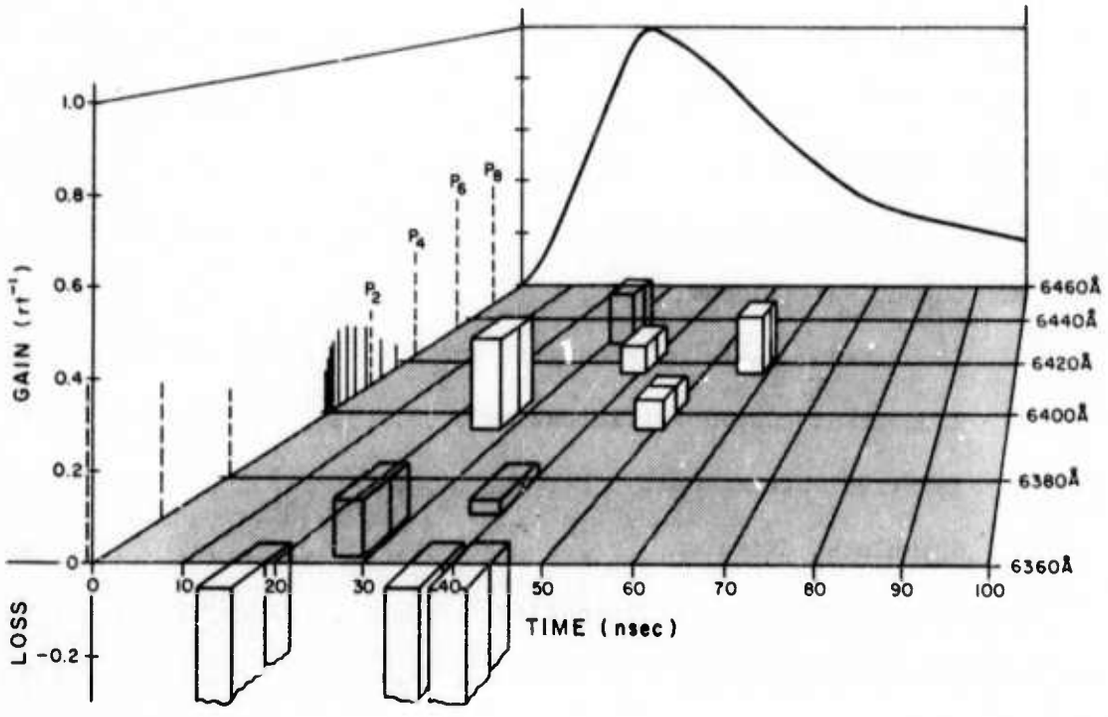

Figure 1

Fractional gain per round trip transit as a function of wavelength and time for the afterglow of a 3 atmosphere helium discharge as directly measured from the enhancement of a probing dye laser beam. Regions of stimulated emission lie above the x,y plane; absorption below. Across the x,z plane to the rear of the data has been plotted the time dependence of the spontaneous emission for scale and on the plane to the left edge is shown the normal emission spectrum of the $3s\,^3\Sigma_u^+ \rightarrow 2p\,^3\Pi_g$ transition of the He_2 uncorrected for broadening mechanisms.

I. TECHNICAL REPORT SUMMARY

The objective of the research described in this report is to determine the feasibility of developing a recombining electron beam-excited plasma into a pulsed laser of exceptionally high peak power. Currently accepted theory supported by the results of this contract research to date indicates this should be possible. Stimulated emission has now been observed in 3 atmospheres of helium and, as seen in the facing figure, gains of the order of 0.04 cm^{-1} have been found by directly measuring the time-resolved amplification of a tunable dye laser beam used to probe the plasma. Power extractions of the order of 5MW/liter have been accomplished with no evidence of saturation of the medium, and indications are encouraging for the prospect of similar activity in related bands of He_2 at 5130, 4400 and 4000 Å. These results confirm the importance of the collisionally-stabilized recombination mechanism as a source of population inversion of significance to the development of new types of high energy lasers depending upon electron beam excitation at high gas densities.

Although a wide variety of recombination processes are known to occur in gaseous plasmas, it is the relatively complex and unfamiliar collisionally-stabilized one which appears to hold outstanding promise as a lasing medium. As discussed in Section II, this process is optimized at high charge densities and relatively low energies but is almost completely quenched in atomic and molecular systems which can participate in dissociative recombination. Theory predicts that, in helium at charge densities of the order of $10^{16} cm^{-3}$, collisionally-stabilized recombination should produce large inverted populations of the resulting neutrals which would tend to radiate in the 2.0μ to 0.3μ wavelength region, provided the temperature of the electron swarm is kept low. It is this requirement which suggests that, unlike conventional visible and UV lasers

excited by electron beams such as the N_2 and H_2 lasers, the lasing action from recombination would be optimized in the afterglow period following the termination of the beam. There is a considerable advantage in this from the viewpoint of fundamental collision cross-sections. In the conventional, directly-excited visible and UV systems, over 95% of the beam energy is lost to the production of ionization not contributing to the laser output. In contrast and as detailed in Section II, theory has predicted that the subsequent collisionally-stabilized recombination of the ions with electrons could provide a mechanism for recovering some of this ionization energy with a resulting order of magnitude increase in the optical output. In this respect, the present system resembles the excimer lasers such as the xenon laser in that high total efficiencies are expected. Unlike these systems, the recombination step is collisionally stabilized thereby introducing an additional dependence on electron temperature and density which offers the prospect of controlling the time-dependent radiative economy through these parameters.

Since both the available output energy and pulse duration depend strongly on the electron density, the high values which only become available from e-beam excitation at high neutral gas pressures are needed. In this requirement lay the basic uncertainty in the approach since previous investigations of this type of charge neutralization had centered on neutral gas densities some 200 times less than the 20 atmosphere values which theory requires for significant radiative output.

The research effort reported here and in previous technical reports[1,2] has focused upon this recombination approach, and the intent of the initial considerations had been to first provide additional tests of theory in helium at intermediate pressures around three atmospheres. From there could be directly determined the amount of light output, the lifetime of the recombination process, and whether or not population inversions were developed.

During the current reporting period, an electron beam-excited helium afterglow system, operating routinely at 5 atmospheres and capable of modification to 20, was instrumented so that spectroscopic observation of transient emissions, both spontaneous and stimulated, in the visible and near IR region could be made with 10 nanosecond resolution. A tunable dye laser was incorporated into the experimental system for the direct measurement of gain through observation of the time-dependent amplification or attenuation of the dye laser beam when passed through the discharge afterglow. Construction details and system performance are presented in Section III.

Technical results discussed in Section IV appear highly encouraging from the perspective of the contract objective. In particular, it was determined that:

1. In the absence of lasing, incoherent emissions of the order of 0.1 to 1.0 milli-Joules/liter per pulse occurred in the afterglow of the 3 atmospheres of helium at 6400 and 5875 Å, respectively. System efficiencies ran as high as 0.04% even without laser action. The efficiency of the recombination process relative to direct excitation of excited states by either primary or energetic secondary electrons was suggested by observation at 3 atmospheres pressure of 0.1 milli-Joule $liter^{-1}$ of spontaneous emission at 6400 Å from the former and less than 0.003 milli-Joules $liter^{-1}$ from the latter.
2. Both the detailed functional forms and effective lifetimes of the spectral transients were consistent with the theory of collisionally-stabilized recombination as applied to an electron swarm at 1000°K effective temperature. Characteristic lifetimes for the recombination source of the radiating populations of He_2 were found to range from 160 nanoseconds at 1 atmosphere of

helium to 26 nanoseconds at 7 atmospheres. The corresponding peak power radiated incoherently at 6400 Å was of the order of 1 KW/liter.

3. Optical gains were examined with two techniques: a) a qualitative survey inferring gain from measurements of time-resolved enhancement ratios of axial intensity emitted from a resonant cavity containing the afterglow and b) by direct measurement of the amplification or attenuation of a pulsed dye laser beam tuned to the wavelength of the transition and transiting the plasma. From the first technique, positive gain was indicated for all transitions examined not terminating on metastable levels. Favorable indications were obtained for bands at 6400, 5130, 4450, and 4000 Å. Use of the tunable laser afforded a resolution of both spectral and temporal behavior of the gain parameters. Preliminary study of the $(3s^3\Sigma_u^+ \rightarrow 2p^3\Pi_g)$ band at 6400 Å showed gain reaching 0.23 per round trip transit at the head of the Q-branch with a time-dependence similar to that of the spontaneous emission.

4. The first estimates of the economy of energy extraction indicated that the energy normally lost during the recombination to non-radiative channels of stabilizations can, in fact, be returned to an induced radiative channel. Energy of the order of 30 milli-Joules/liter and power densities of 5 MW/liter were extracted from the afterglow at 6400 Å with the tunable laser without evidence of saturation of the transition. This value approaches 20% of the maximum energy available theoretically to this transition assuming one photon per ion and reflects favorably upon the feasibility of extracting the energy of one photon from the stimulated transition for each recombination event.

Should theory continue to be validated, the feasibility of the recombination laser would, in fact, be established. In that case, the consequent advantages inherent in the use of the collisionally-stabilized recombination process would be expected to be:

1) Visible to near-UV operating wavelengths. The principal molecular Rydberg series in He_2 extends from 6400 Å to 3680 Å.
2) One output photon per ion. Most of the excitation energy in inert gases goes into ionization and overall efficiencies of 8% should be attained.
3) Lifetimes for the source of population proportional to the inverse cube of the electron density. At 20 atmospheres pressure and an electron density of the order of $10^{16} cm^{-3}$, lifetimes of the order of 1.0 nanosecond should be realized.
4) Scalable output energies. Approximately 5 Joules/liter could be expected at electron densities of $10^{16} cm^{-3}$. At electron densities of $10^{17} cm^{-3}$ which are characteristic of 200 atmospheres pressures, 50 Joules/liter would be expected in a picosecond if the same electron temperature were maintained.
5) Control of the precise temporal form of the output pulse. This can be controlled in principle by heating the recombining electrons and thus varying the rate of the population supply through its expected $T_e^{-9/2}$ dependence.

Evidently, the critical point in the course of this research has been successfully attained in that stimulated emission has been obtained in the 6400 Å band of He_2 with the consequent extraction of significant energy from the afterglow. The task for the immediate future lies in the further confirmation of these results and their extension to other related bands of He_2. With the projected construction of a 100 GW electron beam device (APEX) lasing action

should be realized in one of the bands. Subsequent optimization would then be dependent upon further extensive research into the detailed steps and thermal economy of the recombination process.

II. INTRODUCTION AND REVIEW

Theory[3,4,5,6,7] predicts the occurrence of extremely large inversions of populations in certain recombining high pressure plasmas. However, prior to the commencement of the research contracted in this project, such inversions had only been examined in low pressure helium afterglows. Indications based on those studies of collisionally-stabilized recombination were that it could, in fact, form the basis for a new type of laser of high power. In such a device, the inversion of population would be produced as a consequence of particular ion-electron recombination processes in which the excited atomic or molecular states are sequentially populated, energetically speaking, from the top down. Although theory had predicted substantial consequent pair inversion ratios for almost a decade[7], the difficulties in obtaining recombination controlled plasmas of large volume, which at the same time were free from the competing effects of dissociative recombination, generally prevented the actual observation of such inversions.

The process of collisionally stabilized recombination is a complex one occurring in two composite steps, 1) capture of an electron by an ion and 2) subsequent stabilization. For example, in helium the sequences are the following:

Capture processes

$$He^+ + 2e \rightleftarrows He^*(p) + e$$

$$He^+ + He + e \rightleftarrows He^*(p) + He$$

$$He^+ + e \rightarrow He^*(p) + h\nu$$

Stabilization processes

$$He^*(p) + e \rightleftarrows He^*(q) + e \qquad p > q$$

$$He^*(p) + He \rightleftarrows He^*(q) + He \qquad p > q$$

$$He^*(p) \rightarrow He^*(q) + h\nu \qquad p > q$$

where He*(p) denotes an excited helium atom with principal quantum number, p.

The net result of the initial capture sequence is the establishment of a quasi-equilibrium distribution of population among the bound states whose ionization potential is less than a few KT for the electron gas. However, the total population within such states is usually small compared to the ion density and does not represent a significant portion of the loss of ionization due to recombination. Subsequent stabilization can occur by successive collisional or radiative processes which tend to move population to states of greater ionization potential. When an element of population has been moved to a level of sufficiently high ionization potential, the rates for the inverse ixcitation processes are negligible, and the stabilization is complete. It is during the course of this latter sequence of steps that substantial inversions of population should be produced.[7]

Of first importance to the evaluation of collisional radiative recombination as a process for populating inversions in a practical laser medium are its potential in terms of a) output wavelength and pulse energy, b) pulse duration, and c) efficiency. Consideration of each is reviewed in the following subsections:

a) Output wavelength and pulse energy -- an estimate for these parameters can be made by recognizing that first for a sufficiently high upper state the nearly degenerate sublevels are in thermal equilibrium at the electron temperature, and secondly that most collision-induced changes of energy level result in only a unit change in principal quantum level.[4] In other words, there is no effective mechanism by which the recombining electrons can avoid the upper state of the stimulated transition. Consequently, the least upper boundary on

the number of transitions per pulse which can be stimulated to emit is the number of recombination events occurring in the afterglow period following each ionizing pulse and plasma. Assuming competing losses of ionization can be suppressed, one photon could be obtained for each electron originally produced. Optimization of the energy available would occur by selecting a transition in a Rydberg series of the atom or molecule with principal quantum number as large as possible without elevating the energy into the "quasi-equilibrium group" of levels mentioned above. In principal, this means a photon of energy a few KT less than the greatest ionization energy found in the class of states having transitions to states with very short radiative lifetimes. Examples are found in Figures 2 and 3 which shows excited state energies for He and He_2, respectively. In the former the most suitable series would be the $n^3F \rightarrow 3^3D$ commencing at 1.87μ and converging at ~8190 Å. In the latter species, He_2, the more favorable series, $np^1\Pi_g \rightarrow 2s^1\Sigma_u$, ranging from 5130Å to 3130Å and $ns^3\Sigma_u^+ \rightarrow 2p^3\Pi_g$ ranging from 6400Å to the convergence limit at 3680Å could be attempted. In these cases, Table I summarizes the consequent peak pulsed energy available in a recombining helium afterglow of 10^{16} electron-ion pairs/cm^3.

Figure 2

Energy level diagram of He. Energies of the excited states have been plotted relative to the ground state which is off-scale to the bottom. Wavelengths of the principal transitions have been indicated.

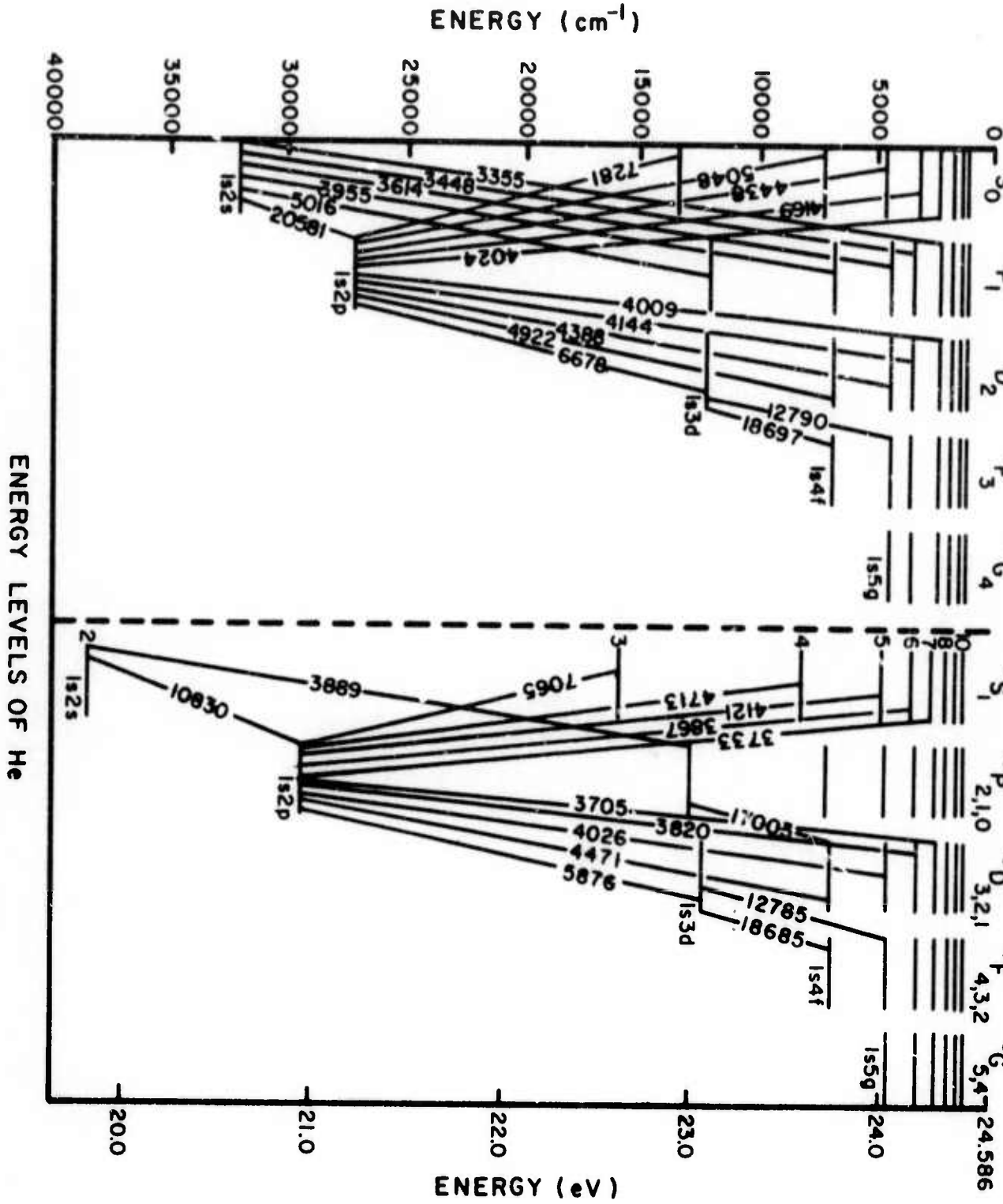
ENERGY (cm⁻¹)
40000
35000
30000
25000
20000
15000
10000
5000
0
1S0
1P1
1D2
1F3
1G4
3S1
3P2,1,0
3D3,2,1
3F4,3,2
3G5,4
1s2s
1s2p
1s3d
1s4f
1s5g
3614
3448
3355
7281
5048
4438
4169
3955
5016
20581
4024
4009
4144
4388
4922
6678
12790
18697
3889
7065
4713
4121
3867
3733
10830
3705
17003
3820
4026
4471
5876
12785
18685
2
3
4
5
6
7
8
ENERGY LEVELS OF He
20.0
21.0
22.0
23.0
24.0
24.586
ENERGY (eV)

Figure 3

Energy level diagram of He_2. Values of energy characteristic of the equilibrium internuclear separation have been plotted relative to the lowest metastable $2s^3\Sigma_u^+$ state. The ground state is $1s\sigma^2 2s\sigma^2$ and strongly repulsive at these internuclear separations. Wavelengths of the band origins of principal transitions have been indicated.

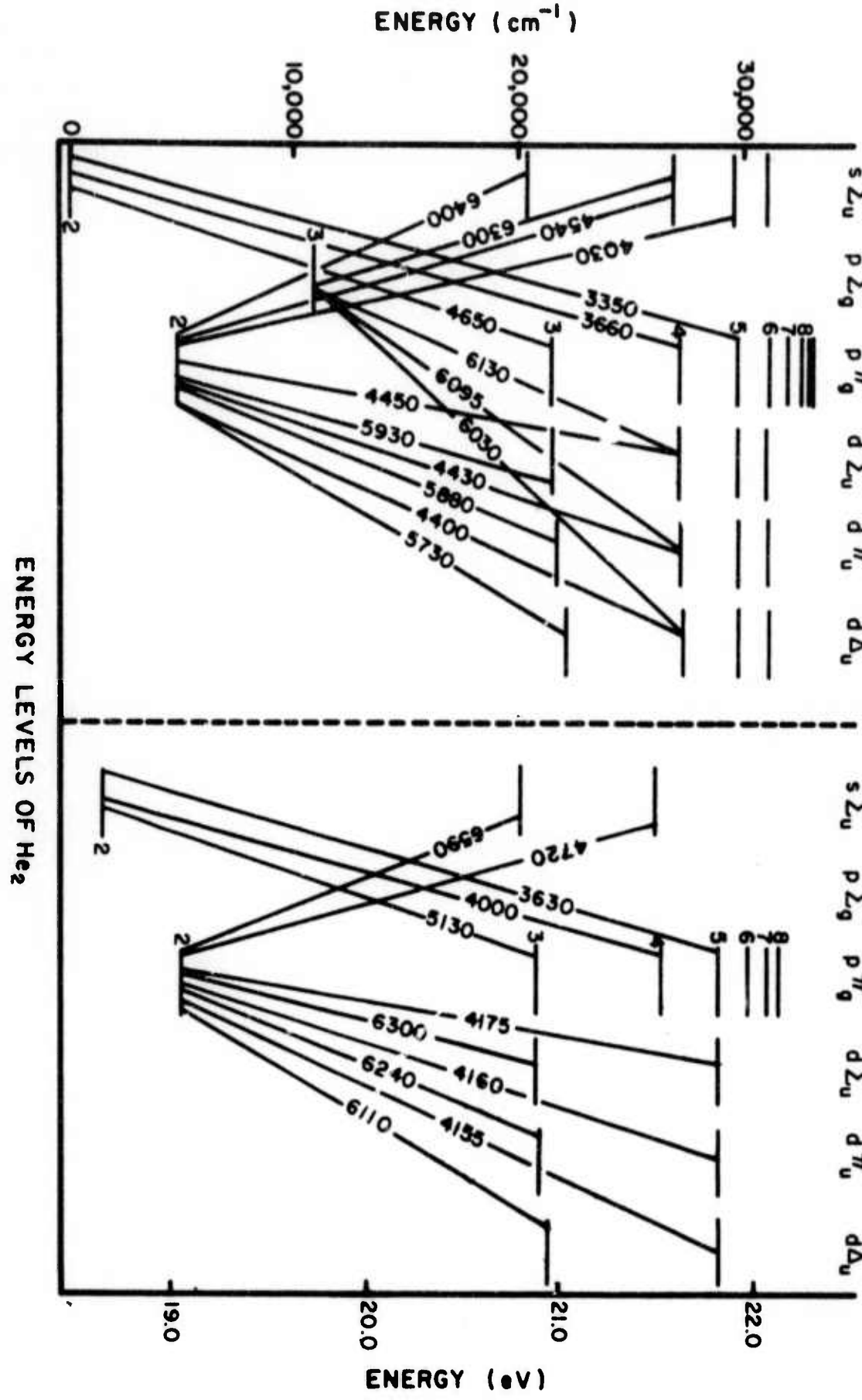
ENERGY (cm⁻¹)
10,000
20,000
30,000
0
2
3
4
5
6
7
8
6400
6300
4540
4030
3350
3660
4650
6130
6095
6030
4450
5930
4430
5880
4400
5730
$s^3\Sigma_u^+$
$p^3\Sigma_g^+$
$p^3\pi_g$
$d^3\Sigma_u^+$
$d^3\pi_u$
$d^3\Delta_u$
6390
4720
3630
4000
5130
4175
6300
4160
6240
4155
6110
$s^1\Sigma_u^+$
$p^1\Sigma_g^+$
$p^1\pi_g$
$d^1\Sigma_u^+$
$d^1\pi_u$
$d^1\Delta_u$
ENERGY LEVELS OF He_2
19.0
20.0
21.0
22.0
ENERGY (eV)

Table I

Peak Pulsed Energies Available in Listed Transitions

Wavelength	Species	State	Quantum Efficiency	Energy (Joule/liter)
18700Å	He	$4^3F \rightarrow 3^3D$	2.7%	1.1
8190Å	He	$\lim n^3F \rightarrow 3^3D$	6.2%	2.4
6400Å	He_2	$3s^3\Sigma_u^+ \rightarrow 2p^3\Pi_g$	8.6%	3.1
5130Å	He_2	$3p^1\Pi_g \rightarrow 2s^1\Sigma_u$	10.8%	3.8
3680Å	He_2	$\lim ns^3\Sigma_u^+ \rightarrow 2p^3\Pi_g$	15.0%	5.4
3130Å	He_2	$\lim np^1\Pi_g \rightarrow 2s^1\Sigma_u^+$	17.7%	6.3

b) Pulse duration -- The pulse duration is more difficult to estimate from theory. In the first approximation, the entire energy available to the lasing transition can be assumed to be emitted in a time comparable to the inverse of the recombination rate. Initially, problems resulted from the paucity of measurements of this rate for collisionally-stabilized recombination. For theoretical reasons, the effective two-body recombination rate coefficient, defined for the ion X^+ by

$$\frac{\partial}{\partial t}[X^+] = -\alpha[X^+][e] \quad , \qquad (1)$$

was expected[4,9] to have the form

$$\alpha = K_e[e]\,(T_e/300)^{-9/2} + K_N[X]\,(T_e/300)^a \qquad (2)$$

where [e] and [X] denote the concentrations of free electrons and neutral atoms respectively, T_e, the electron temperature, and a is a coefficient which is still undetermined at the present time.

Values in the literature[9,10,11] had been somewhat scattered and entirely confined to values of electron and neutral particle densities several orders of magnitude below those now obtainable with beam-excited discharges. In the absence of more appropriate values, the best estimates for He^+ from the literature had seemed to be

$$\alpha \simeq 7 \times 10^{-20}[e](T_e/300)^{-9/2} + 10^{-27}[He] \quad , \qquad (3)$$

and for He_2^+

$$\alpha \simeq 1.5 \times 10^{-20}[e](T_e/300)^{-9/2} + 1.5 \times 10^{-27}[He] \quad . \qquad (4)$$

However, there was some evidence[12] that a more generalized model was necessary and best characterized by

$$\alpha = K[e]^{\eta}(T_e/300)^{-9/2} \qquad (5)$$

where η is a function of pressure and $0 \leq \eta \leq 1$. At 44.6 Torr prior measurements over the range, 10^{10} to 10^{12} cm^{-3}, of electron densities for He_2^+ indicated a value of

$$\alpha \simeq 2.8 \times 10^{-11}[e]^{0.185} \qquad (6)$$

where [e] is again the electron density in units of cm^{-3}.

In either case, an equivalent exponential lifetime against recombination, τ, can be defined to be

$$\tau^{-1} \equiv \frac{1}{[X^+]} \frac{\partial}{\partial t} [X^+] = -\alpha[e] \quad . \qquad (7)$$

The resulting expected lifetimes are summarized in Table II.

Table II

Lifetimes Against Recombination

Species	[e] (cm^{-3})	T_e (°K)	τ (sec)
He^+	10^{16}	300	0.14×10^{-12}
		3000	0.44×10^{-8}
He_2^+	10^{16}	300	1.0×10^{-12}
		3000	3.0×10^{-8}

Superficially, it appears that any lifetime, hence pulse duration could be attained provided 1) the ionization could be produced in a time short compared to the output pulse and 2) the electron temperature could be adjusted to a sufficiently low value in the same time. Unfortunately, the electron temperature is not a free parameter, but had been predicted[13,14] to be controlled by the feedback of energy to the electron gas during the stabilizing collisions between excited states and the free electrons. Current theory[13] had originally indicated that a value in the range 1500°-1800°K would be appropriate for the 10^{16} cm^{-3} electrons in helium at STP. Nevertheless, it must be recognized that such an estimate had been based upon extrapolation of parameters over so many orders of magnitude from measured values as to render the nine-halves power of the

These questions were largely resolved[1,2,15] during the first contract year of this project through the measurement and parametric representation of the functional dependence on time of the intensity of the spontaneous emission. The relevant model for that radiation is obtained by starting from the more general expression for the collisional recombination rate coefficient, equation (5), substituting it into the continuity equation for ion density, neglecting diffusion at these pressures, as well as competing reactions, assuming $[He_2^+] = [e]$, and a

constant $T_e \sim 300°$; then

$$[He_2^+(t)]^{-(1+\eta)} - [He_2^+(0)]^{-1+\eta} = (1+\eta)Kt \quad . \qquad (8)$$

Now it is expected[11] that the rate of spontaneous photon emission in any particular band during the course of the stabilization of the recombination should approximately equal some constant fraction, f, of the recombination rate of the ions which, allowing for geometric collection factors and sensitivities, implies that

$$I(t) = C\,K\,[He_2^+(t)]^{2+\eta} \quad , \qquad (9)$$

where C represents all collected scale factors. Substituting (9) into (8) gives:

$$\frac{I(t)^{-\frac{1+\eta}{2+\eta}} - I(0)^{-\frac{1+\eta}{2+\eta}}}{t} = (1+\eta)(CK)^{-\frac{1+\eta}{2+\eta}} K \quad . \qquad (10)$$

This implies that a plot of intensity to the $-(1+\eta)/(2+\eta)$ power would be a linear function of time and that the slope, S, of such a curve would be simply the right-hand side of (10). Defining then

$$S = (1+\eta)(CK)^{-\frac{1+\eta}{2+\eta}} K \qquad (11)$$

enables the effective lifetime of the collisional recombination defined by equation (7) to be written in terms of experimentally measured parameters as

$$\tau_0^{-1} = \alpha[He_2^+(0)] = S(1+\eta)^{-1} I_0^{\frac{1+\eta}{2+\eta}} \quad . \qquad (12)$$

Examination of this equation in comparison with (11) shows τ_0^{-1} to be independent of the scaling of the intensity as would be expected.

These results suggested the procedure of plotting the inverse intensity to the $(1+\eta)/(2+\eta)$ power for various trial values of η between 0 and 1, determining the best straight line slope, if any, and then obtaining the recombination lifetime from (12). This was accomplished experimentally in an extensive series of measurements recently reported[2,15] and briefly reviewed below for convenience.

In practice, these measurements were greatly facilitated in both speed and accuracy by interfacing a Biomation 8100 transient recorder to the on-line data acquisition computer serving the University's Atomic Physics group. A digital image of each decay curve of spontaneous intensity could be stored and the required inverse intensity to the various fractional powers plotted. Typical data for the principal spectral features of He_2 at 6400 Å and 4650 Å for afterglows at the three pressures, 1, 3, and 4.2 atmospheres in the HPAC-1b system are shown in Figures 4 and 5, together with the resulting computer analyses and plots.

Lifetimes of the two molecular features, 6400 Å and 4650 Å, show reasonable agreement over the range of pressures examined and suggest the validity of the assumption summarized in equation (9) that the emitted intensity is a constant fraction of the energy released by the recombining He_2^+ ions.

The converse behavior was found for the recombination portion of the decay of the atomic lines examined. Lifetimes deduced did not agree with the recombination rates for the molecular bands or even with each other. The most extreme divergence was shown by the $3^3D \rightarrow 2^3P$ transition at 5875 Å which is reproduced in Figure 6.

The lifetime is anamolously long as can be seen upon inspection, and consists of two slopes as shown in the corresponding analyses which present the inverse intensities for various η. Other atomic lines did not show the two lifetime behavior but did show scattered lifetimes.

Figure 4

Three data plots showing the time evolution and its analyses of the 6400 Å emission in the afterglow from single discharges of the e-beam, sequentially at 1, 1, and 4.2 atmospheres pressure in the HPAC-1b system. Each page shows, counter-clockwise from the upper left,

a) Photograph of the refreshed oscilloscope trace of the analog reconstruction of the stored transient.
b) Plot of the digital image of the stored transient.
c) Plot of the inverse intensity to the M-power as a function of decay time for η=0, neutrally stabilized recombination.
d) Plot of the inverse intensity to the M-power as a function of decay time for η=1, electronically stabilized recombination.

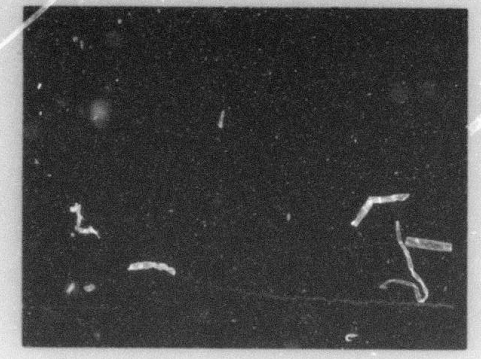

Scale: 40 nanoseconds per horizontal division
0.05 Volts per vertical division

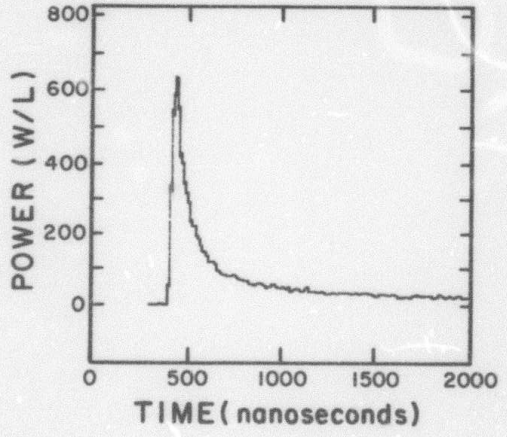

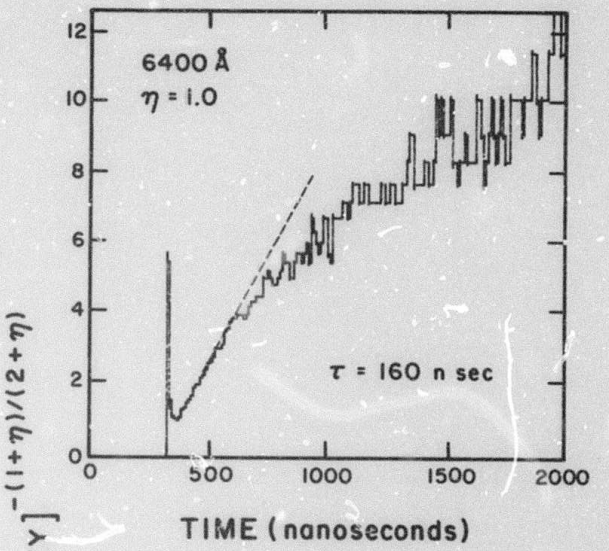

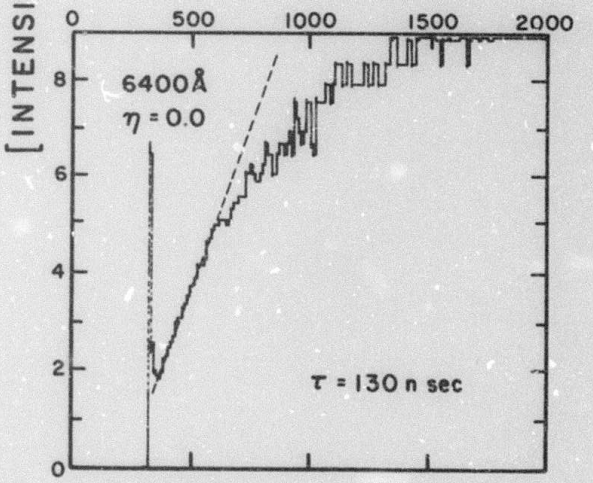

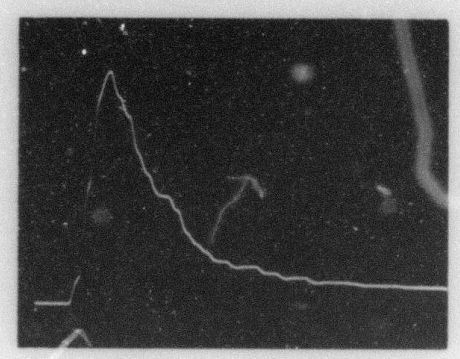

Scale: 40 nanoseconds per horizontal division
0.05 Volts per vertical division

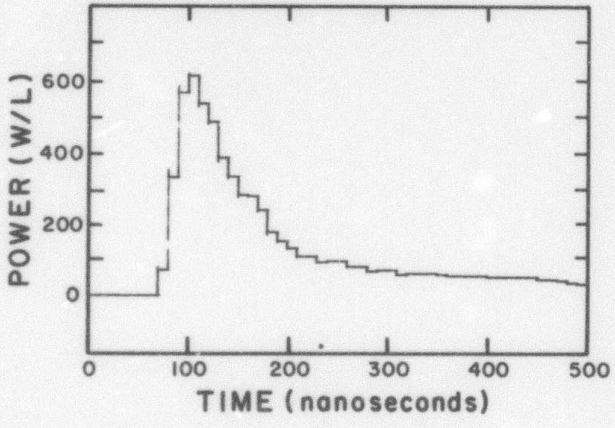

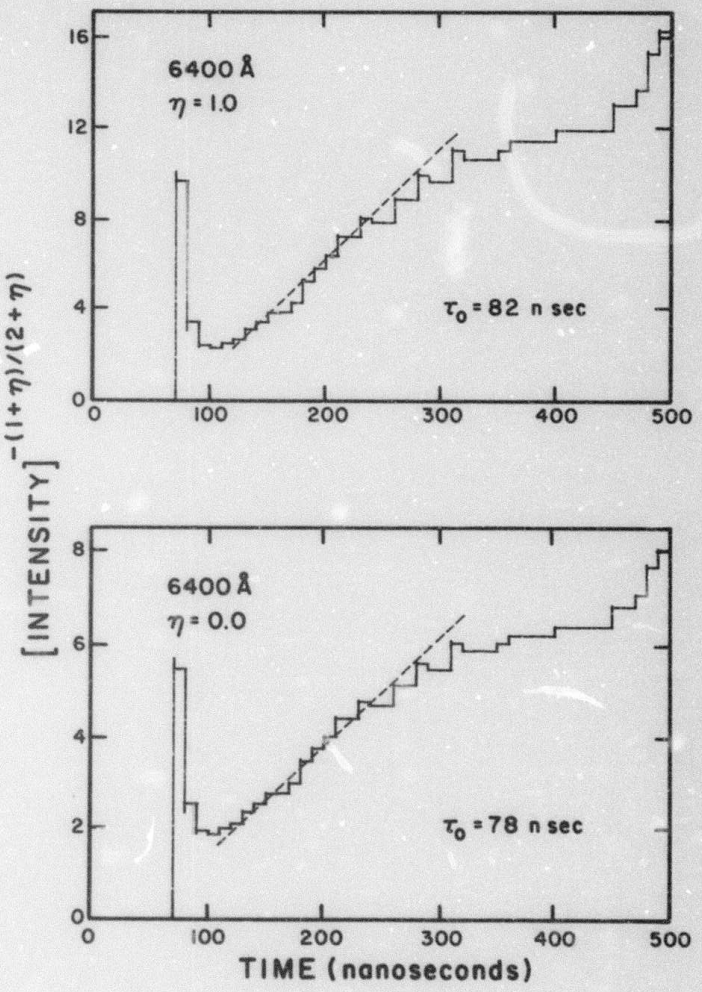

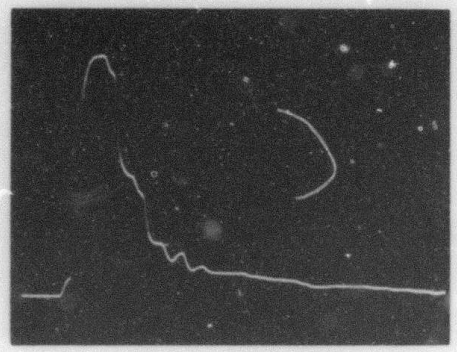

Scale: 200 nanoseconds per horizontal division
0.05 Volts per vertical division

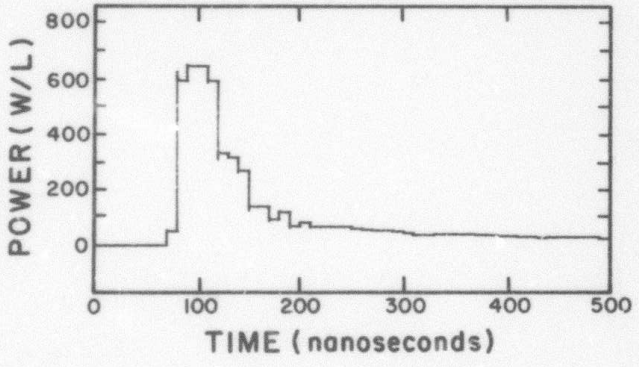

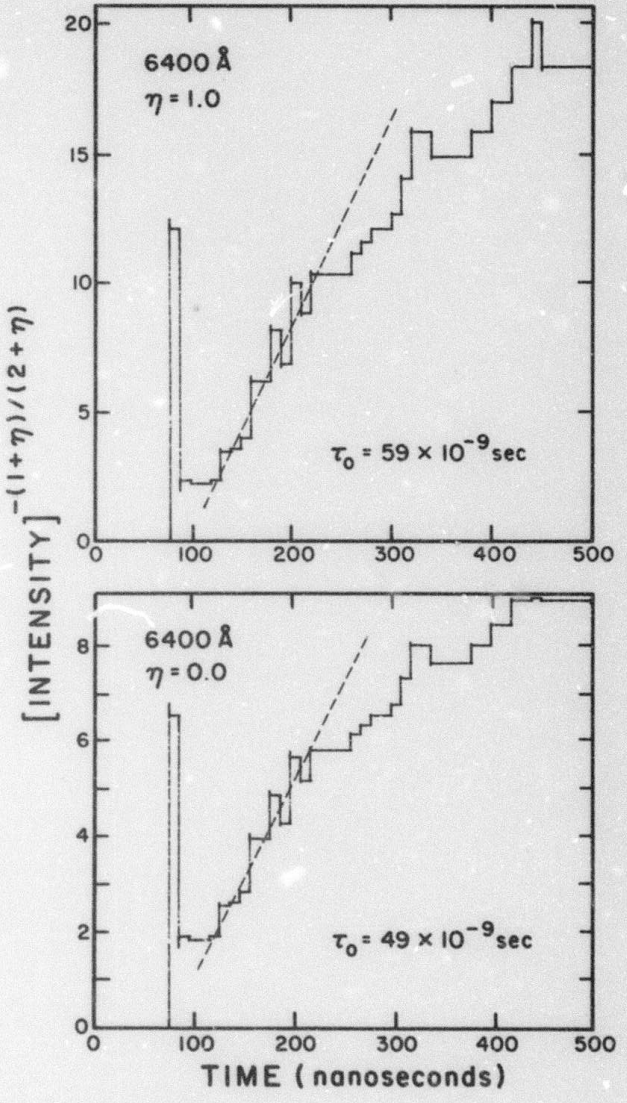

Figure 5

Three data plots showing the time evolution and its analyses of the 4650 Å emission in the afterglow from a single discharge of the e-beam, sequentially at 1, 3, and 4.2 atmospheres pressure in the HPAC-1b system. Each page shows, counter-clockwise from the upper left,

a) Photograph of the refreshed oscilloscope trace or the analog reconstruction of the stored transient.
b) Plot of the digital image of the stored transient.
c) Plot of the inverse intensity to the M-power as a function of decay time for $\eta=0$, neutrally stabilized recombination.
d) Plot of the inverse intensity to the M-power as a function of decay time for $\eta=1$, electronically stabilized recombination.

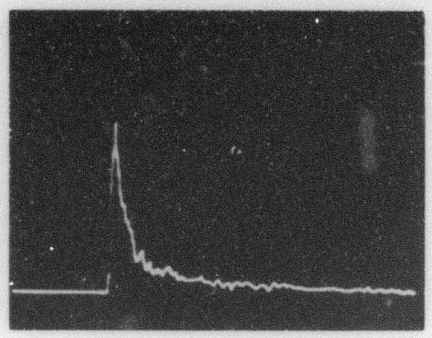

Scale: 200 nanoseconds per horizontal division
0.025 Volts per vertical division

24.

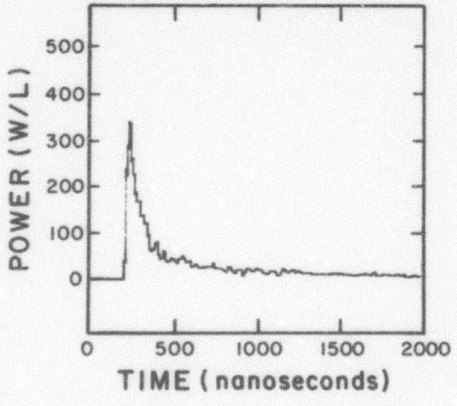

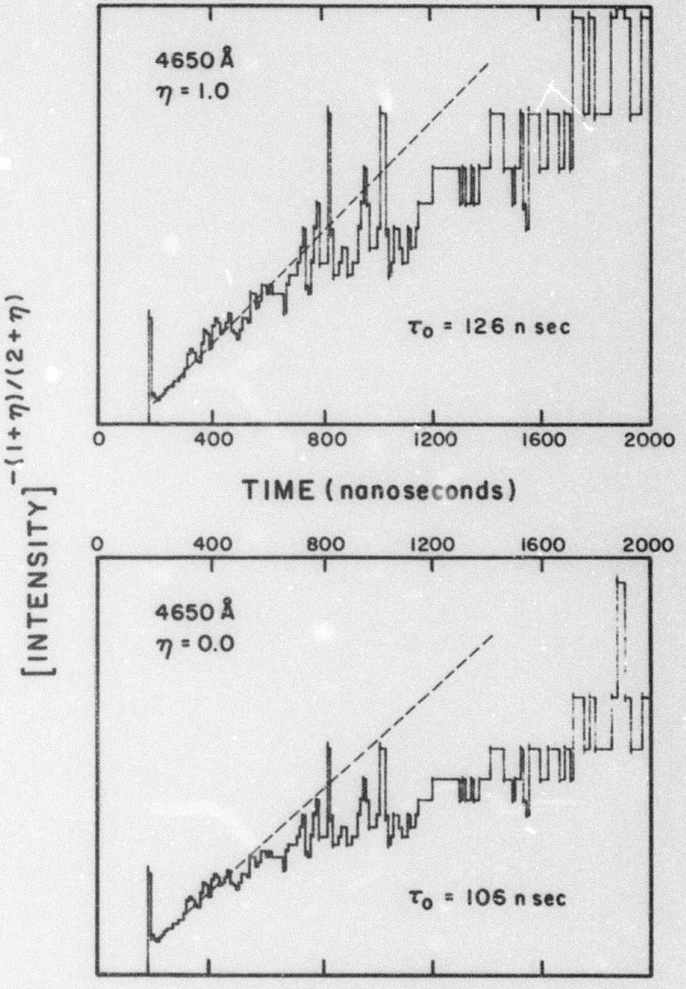

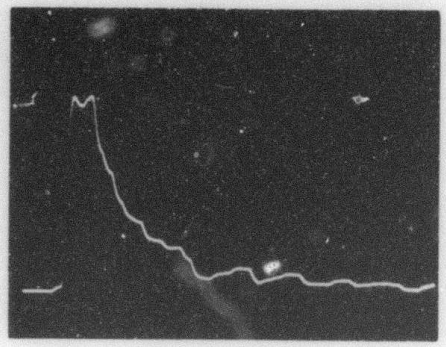

Scale: 40 nanoseconds per horizontal division
0.025 Volts per vertical division

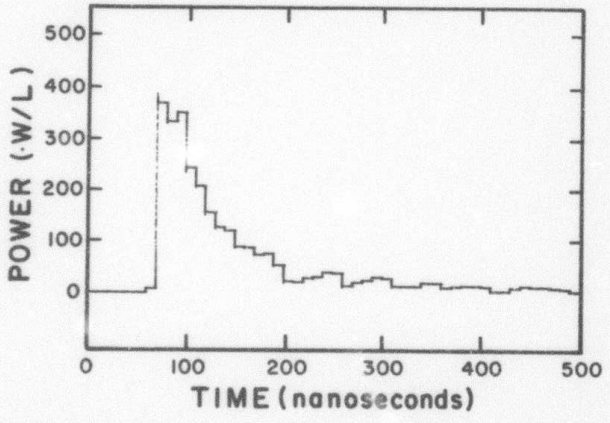

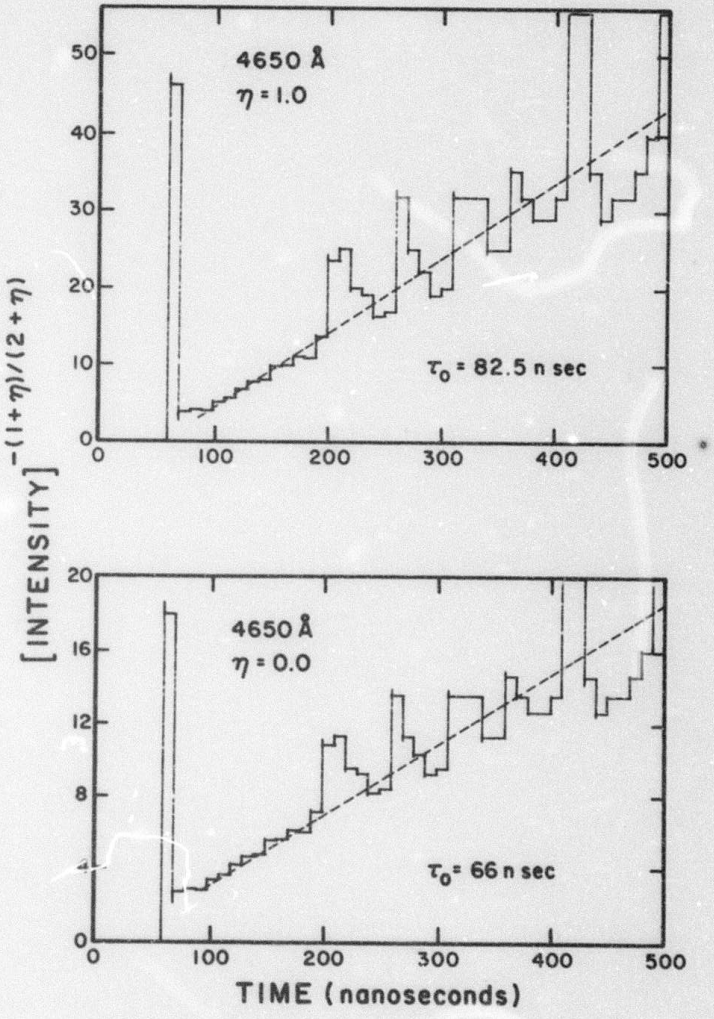

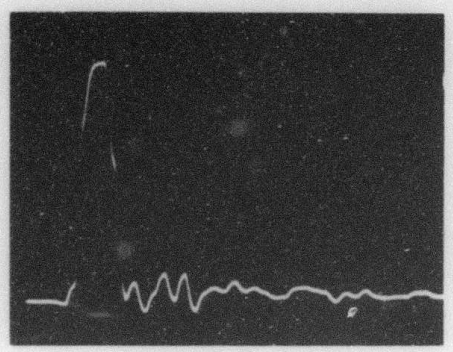

Scale: 40 nanoseconds per horizontal division
0.025 Volts per vertical division

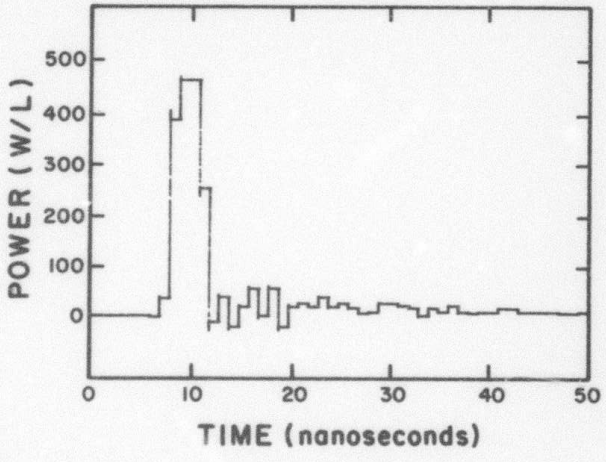

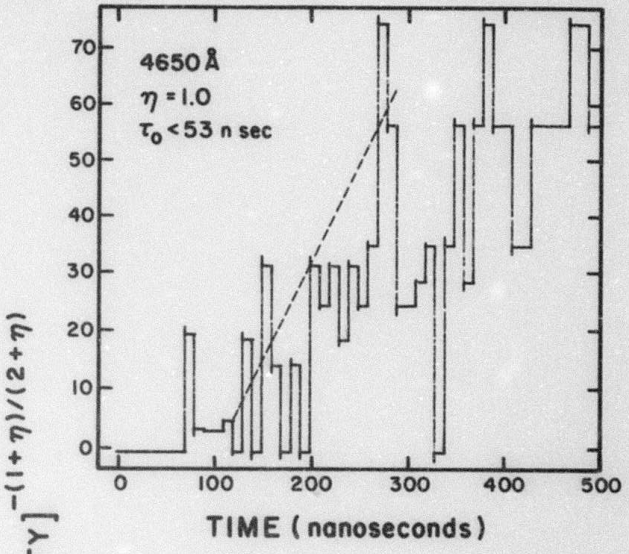

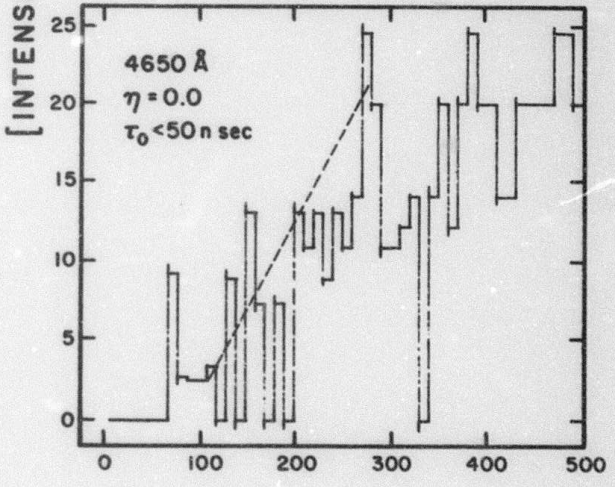

Figures 6

Three data plots showing the time evolution and its analyses of the 5875 Å emission in the afterglow from a single discharge of the e-beam, sequentially at 1, 3, and 4.2 atmospheres pressure in the HPAC-1b system. Each page shows, counter-clockwise from the upper left,

a) Photograph of the refreshed oscilloscope trace of the analog reconstruction of the stored transient.
b) Plot of the digital image of the stored transient.
c) Plot of the inverse intensity to the M-power as a function of decay time for η=0, neutrally stabilized recombination. Plot of the inverse intensity to the M-power as a function of decay time for η=1, electronically stabilized recombination.

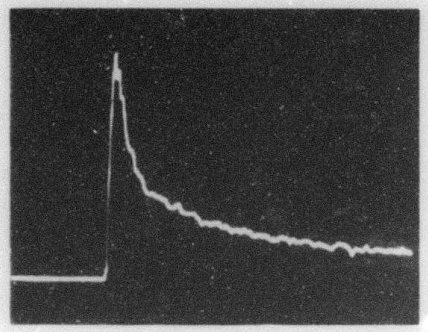

Scale: 200 nanoseconds per horizontal division
0.05 Volts per vertical division

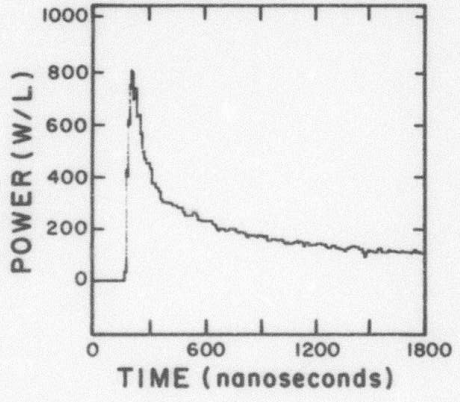

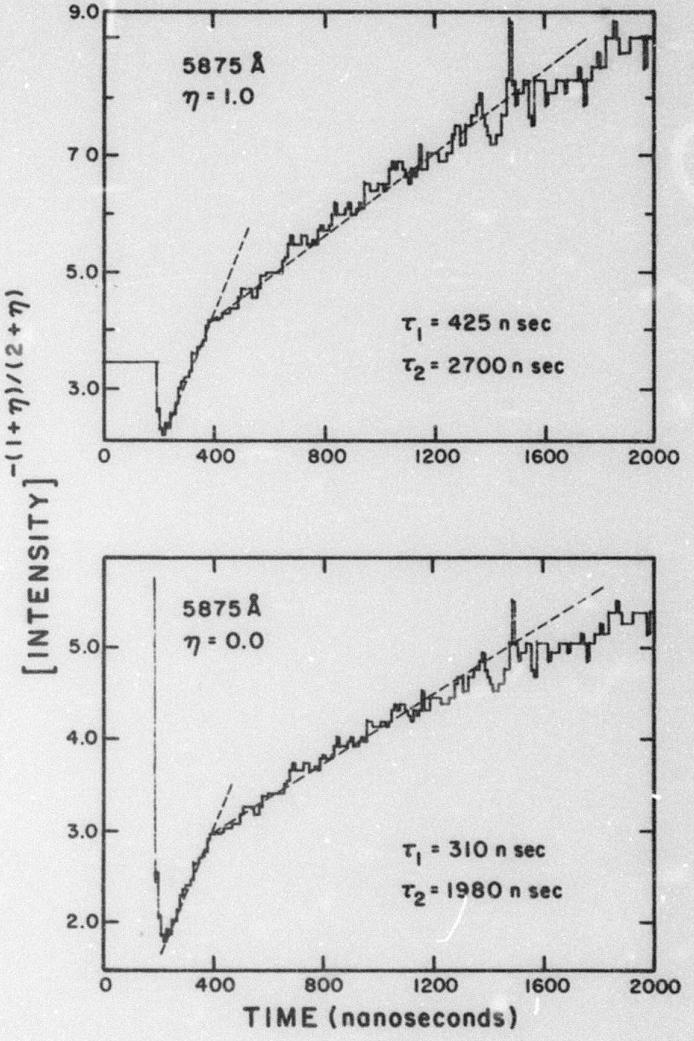

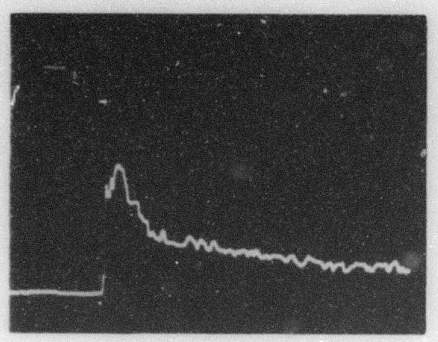

Scale: 200 nanoseconds per horizontal division
0.025 Volts per vertical division

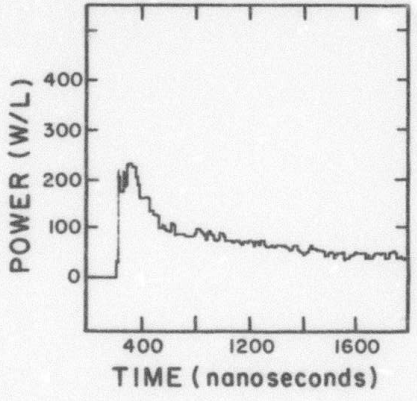

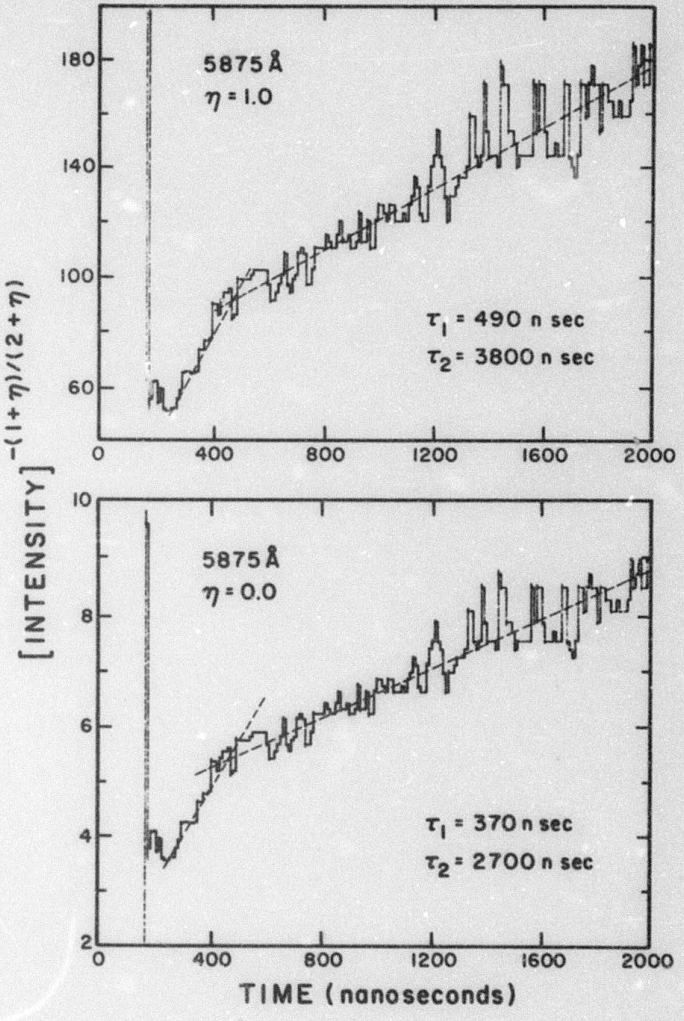

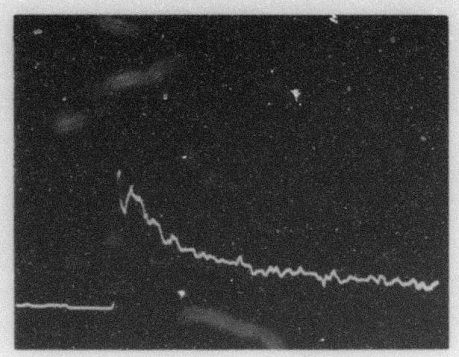

Scale: 200 nanoseconds per horizontal division
0.025 Volts per vertical division

30.

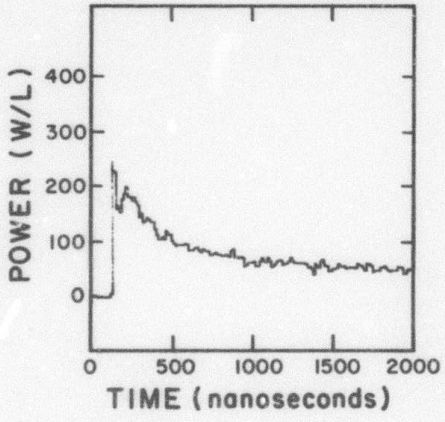

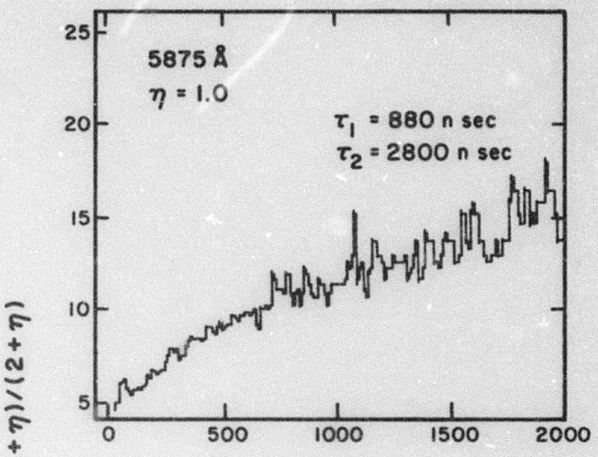

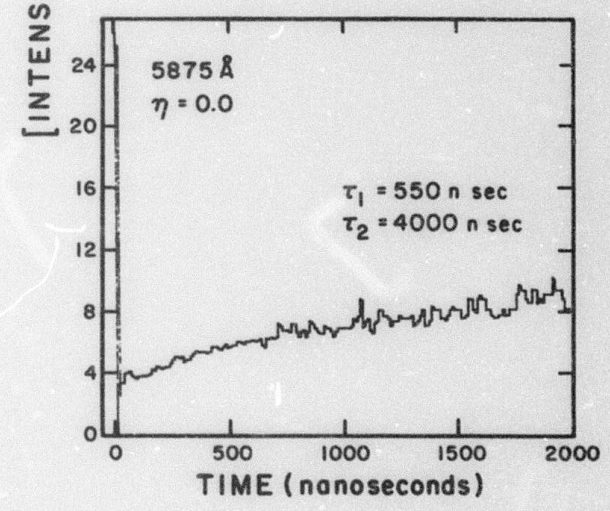

The rather extreme variation of atomic recombination lifetimes strongly indicates that, for the production of excited atoms, the assumption expressed by (9) does not hold and that the relative importance of the various stabilizing channels is a changing function of electron density and hence, time. This is in general agreement with the results of 0.1 atmosphere work which has demonstrated that the molecular bands tend to have the same time decays[12] in agreement with (9) while the atomic lines do not[11].

Results for the He_2^+ recombination lifetimes are collected in Table III and presented graphically in Figure 7.

Table III

Summary of Lifetimes of the Principal Spectral Features

Wavelength	Lifetime η=1 (nanoseconds)			
Pressure (atm)	1	3	4.2	7
He_2				
6400 Å	160	82	59	26*
4650 Å	126	82.5	53	34*
He				
7065 Å	-	267	350*	93*
6678 Å	208*	100*	45*	29*
5875 Å early	880	490	425	300*
late	2800	3800	2700	2320*

*HPAC-2 system

These results evidently agree with expression (4) for an electron temperature which is a weak function of pressure and has a value around 1000°K at 3 atmospheres.

Figure 7

Lifetimes of the sources of population of states resulting from the collisionally stabilized recombination of helium ions produced by the e-beam. Experimental values at different pressures are shown by open circles and theoretical values by solid bars. Values are marked on the bars which correspond to the electron temperatures indicated.

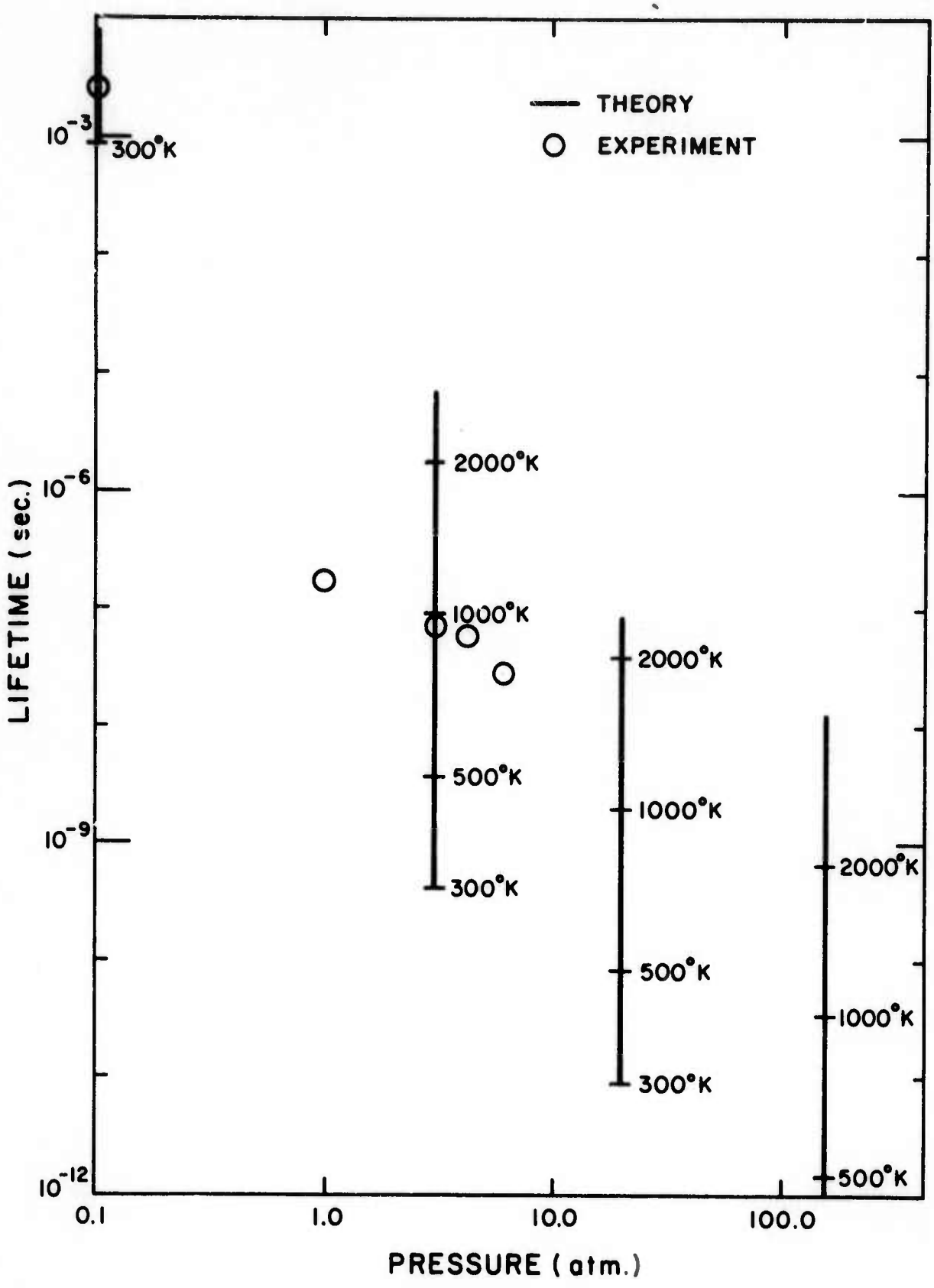
THEORY
EXPERIMENT
10^{-3}
300°K
10^{-6}
2000°K
1000°K
500°K
10^{-9}
300°K
2000°K
1000°K
500°K
300°K
2000°K
1000°K
500°K
10^{-12}
LIFETIME (sec.)
0.1
1.0
10.0
100.0
PRESSURE (atm.)

c) Efficiency -- Although the quantum efficiencies summarized previously in Table I are not extremely impressive, the system efficiencies expected for a recombination laser should be limited primarily by these quantum efficiencies. This results from an exceedingly effective use of electron beam energy. Whereas in many e-beam excited laser systems, including N_2 and H_2, waste of over 90% of beam energy lost in inelastic collisions occurs in the production of ionization as opposed to excitation, in the recombination scheme, use is directly made of that ionization. Considering that about 42.3eV of beam energy is expended in the production of a 24.5eV He^+ ion or 22.4eV He_2^+ ion, system efficiencies of 58% and 53%, respectively, of the quantum efficiencies should be attainable. This implies that recombination lasers should achieve overall efficiencies of 5 to 10 percent. Preliminary measurements discussed in Section IV on the economy of energy extraction tend to support this estimate.

III. EXPERIMENTAL METHOD

The objective of this program has been stated to be the evaluation of the potential utility to laser development of recombining high pressure helium plasmas. Although there are several ways in which this could have been done, the paucity of data existing prior to the initiation of this contract research necessitated an initial survey and characterization of the afterglow properties in order to develop a model to guide understanding. As discussed in the previous section, even theory provided little assistance, being extrapolated to parameter values over two orders of magnitude beyond prior experimental verifications.

The initial approach consisted of three steps. First, a survey of the spectrum of spontaneous emission was planned to identify which excited species and states could be found under the various experimental conditions of pressure and electron density. Second, an investigation of the time-resolved decay of spontaneous emission was intended from which relevant rate coefficients for recombination and de-excitation could be obtained. Finally, measurements of the potential gain of the various promising transitions identified in the preceeding were planned to guide the study of any stimulation emissions which might be expected and prepare the way for quantative measurement of the resulting radiative economy. It has been essentially this course which has been followed, as reported in this and previous technical reports.[1,2]

To support this research, a sophisticated ultra-high vacuum and gas handling system was constructed and used to prepare and fill several different designs of high-pressure afterglow chambers(HPAC). System integrity was found to be of great importance because of the high ionization potential of the helium ions and their large cross-sections for charge transfer to impurity gas atoms and molecules. Figure 8 schematically outlines the functions of the gas handling system. All standard components were Varian 2 in. UHV grade.

Figure 8

Schematic representation of the UHV vacuum and associated gas handling systems. The dotted lines enclose portions bakeable to 400°C. The dashed lines enclose additions to the system to be implemented when HPAC-2 was installed and used subsequently with HPAC-1b.

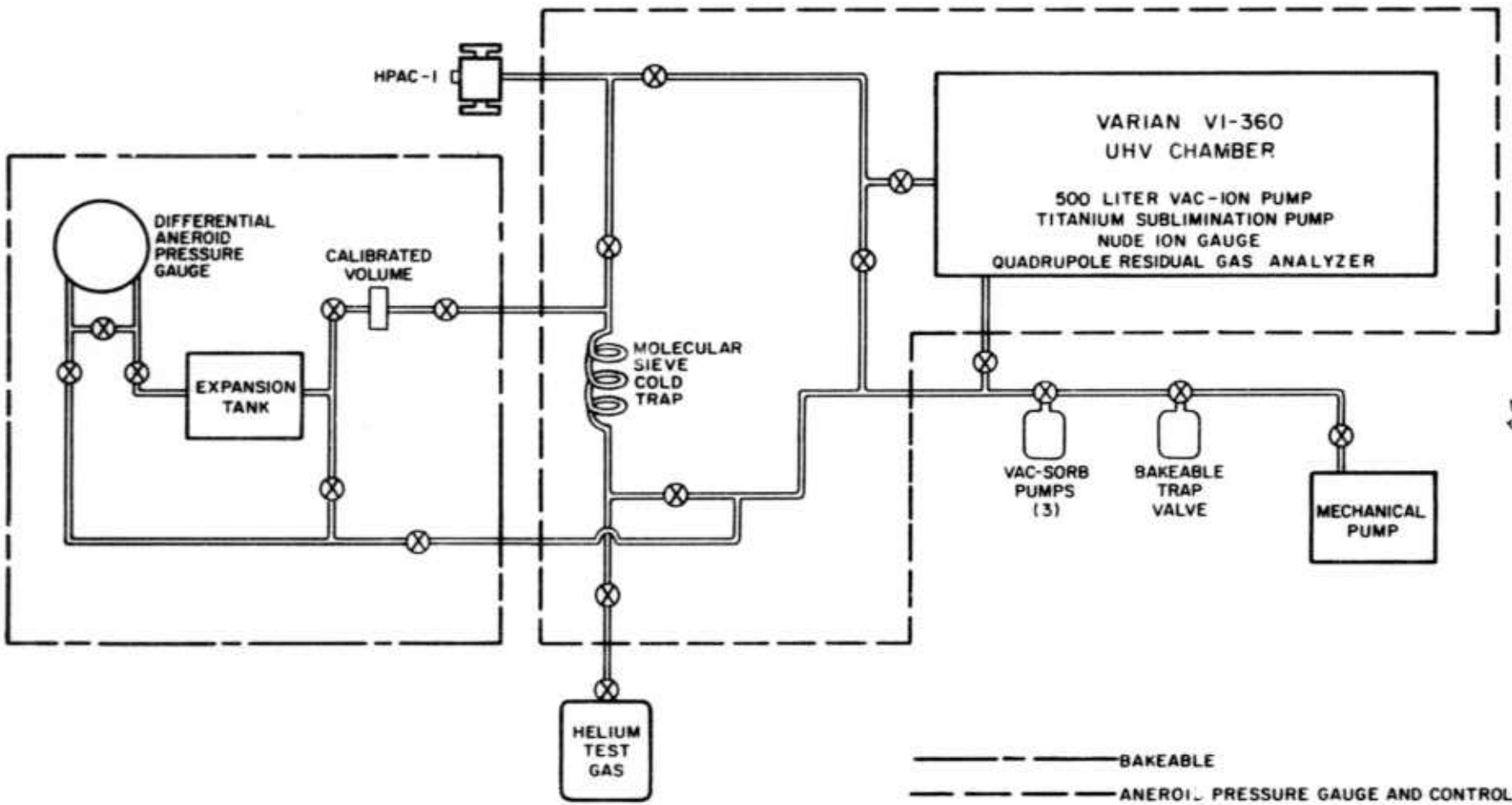
HPAC-1
VARIAN VI-360
UHV CHAMBER
500 LITER VAC-ION PUMP
TITANIUM SUBLIMINATION PUMP
NUDE ION GAUGE
QUADRUPOLE RESIDUAL GAS ANALYZER
DIFFERENTIAL
ANEROID
PRESSURE
GAUGE
CALIBRATED
VOLUME
EXPANSION
TANK
MOLECULAR
SIEVE
COLD
TRAP
VAC-SORB
PUMPS
(3)
BAKEABLE
TRAP
VALVE
MECHANICAL
PUMP
HELIUM
TEST
GAS
BAKEABLE
ANEROID PRESSURE GAUGE AND CONTROLS

The portion enclosed in dotted lines was bakeable to 400°C while the part in dashed lines was an addition implemented with HPAC-1b to provide accurate pressure measurement without contamination.

System integrity was such that, after a mild bakeout with heating tapes, a pressure of 3×10^{-11} Torr could be maintained in the dump tank while the valve to HPAC-1b was open. Final verification was obtained with a commercial helium leak detector which failed to show any detectable leaks.

Figure 9 shows a drawing of the afterglow chamber HPAC-1b. It is basically a welded stainless steel box having the schematic form of a horizontal cross with an additional downward leg serving as an inlet port. One pair of opposed arms is terminated by gasketed windows and the other pair contains the pumping port opposite to the e-beam window. Dimensions and construction details are found in the figure. Windows were either quartz fused through graded seals to Varian flanges, or sapphire directly mounted in Varian flanges.

Residual gas analysis was performed after each evacuation and showed only traces of contaminant. A typical mass spectrum is shown in Figure 10a.

After evacuation, the chamber was valved off from the pump and filled through the inlet port with helium of high initial purity, further conditioned by passing it at the fill pressure through a molecular sieve trap cooled to liquid nitrogen temperatures. Bureau of Mines analyses of cylinders of similar grade have shown one or two ppm non-condensable, inert (neon) impurity, and it is believed that this figure represents the ultimate purity attainable with this system. As will be discussed in the following section, this treatment sufficed to reduce all impurities below the threshold of spectroscopic detection by optical means. Typical mass spectrometric analysis of the cell contents at the completion of an experimental sequence is shown in Figure 10b. No evidence of leakage or gas evolution can be detected. Nevertheless, should

Figure 9

Drawing of the High Pressure Afterglow Chamber, Version 1b (HPAC-1b) showing construction details.

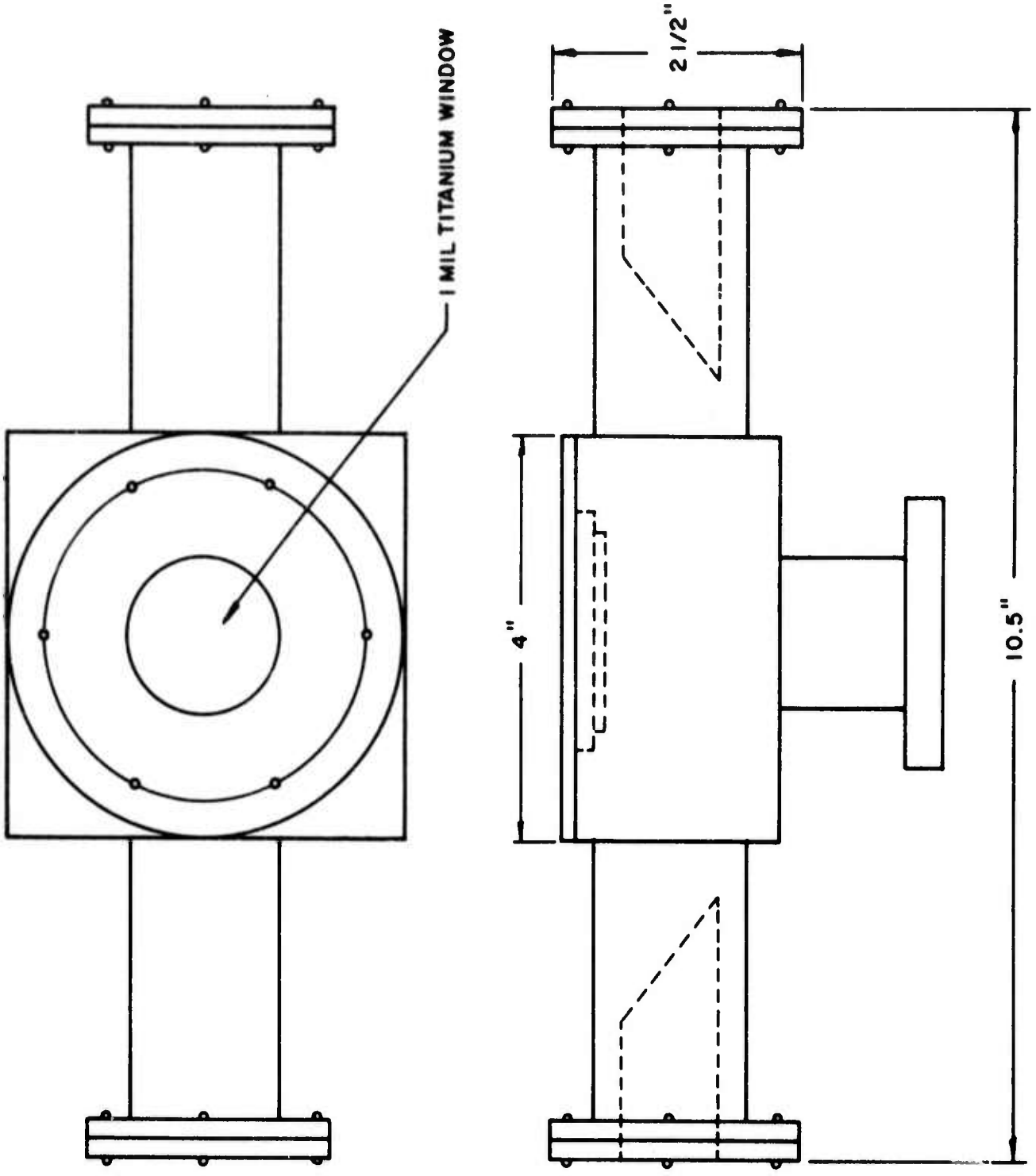
1 MIL TITANIUM WINDOW
2 1/2"
4"
10.5"

Figures 10

Residual gas analysis obtained after evacuation of HPAC-1b

a) Mass spectrum of steady state evacuation, initial condition before filling with helium.

b) Mass spectrum of cell contents after an experimental cycle of the order of 4 hours and 50 e-beam discharge pulses.

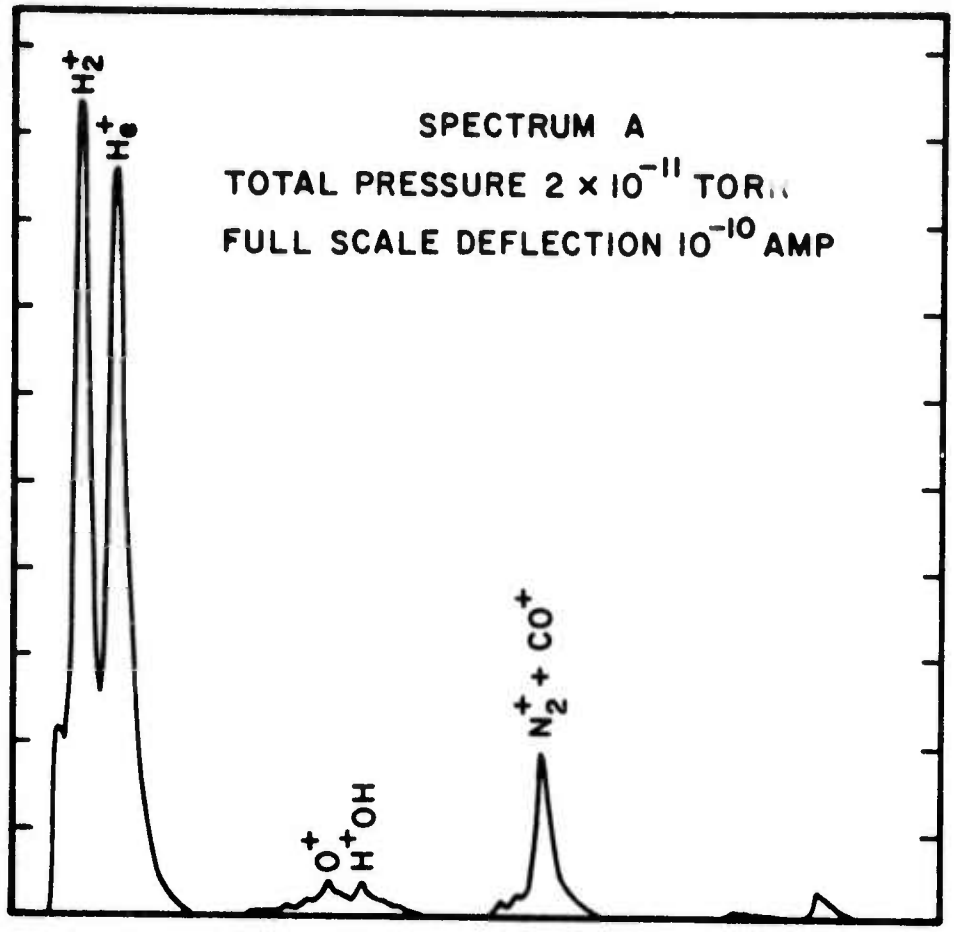
SPECTRUM A
TOTAL PRESSURE 2 x 10^-11 TORR
FULL SCALE DEFLECTION 10^-10 AMP
+H2
+He
+O
+OH
+N2 + CO+

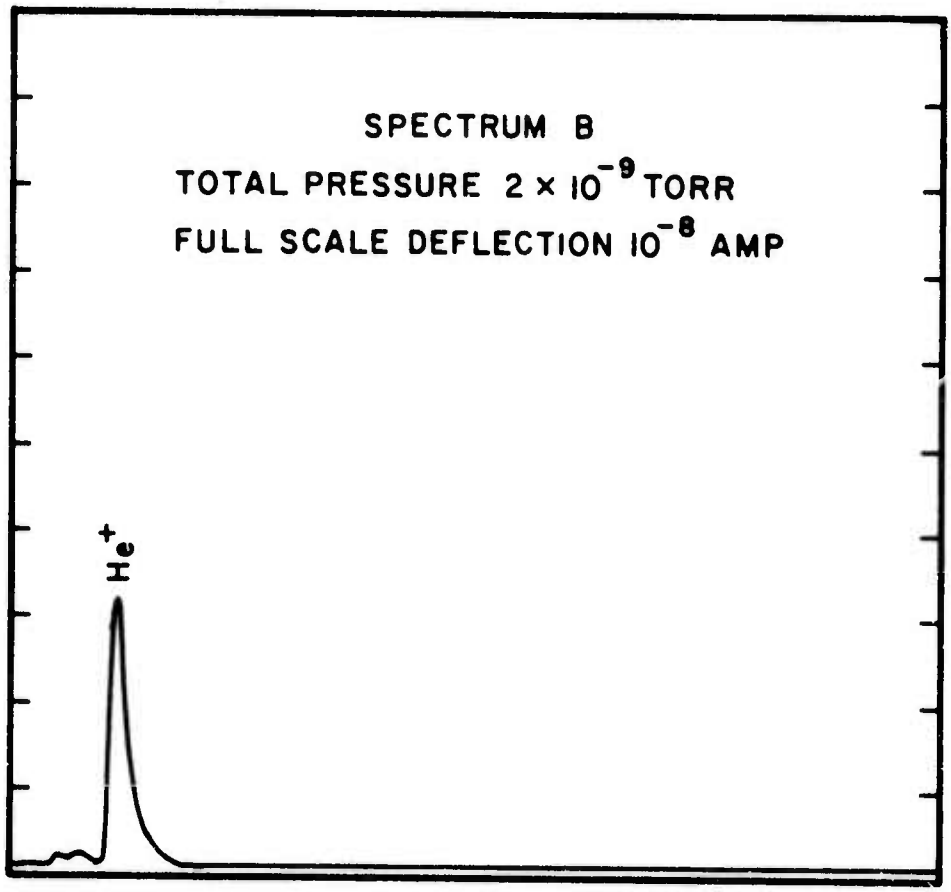
SPECTRUM B
TOTAL PRESSURE 2 x 10^-9 TORR
FULL SCALE DEFLECTION 10^-8 AMP
He+

the need arise in future stages, several cylinders of <0.2ppm inert impurity have been obtained. Further improvement to parts in 10^9 can be achieved if necessary through low-pressure cataphoresis followed by recompression. The latter is a tedious and expensive step and will be implemented only if necessary.

In the cell, the primary ionization is produced by a nominal 0.5 MeV electron beam entering the HPAC through a 0.001 inch thick titanium foil. The beam is produced by a Field Emission Corp. 706 e-beam gun which can emit 2×10^{14} electrons per 3-nanosecond pulse. Divergence of the beam is reported to be 30° so that, at a distance ℓ, normal to the window, there can be expected to be

$$N_p = 1.5 \times 10^{14}[1 + 0.81\ell + 0.165\ell^2]^{-1} \quad , \quad (13)$$

primary electrons per cm^2 incident upon the HPAC beam window. From values of average range, energy expended per ion-electron pair, and gas density, an average charge multiplication factor in helium of

$$M = 15.6 \text{ cm}^{-1}\text{atm}^{-1} \quad , \quad (14)$$

can be computed.

The preliminary diagnostic data obtained with HPAC-1 and discussed in the following section was obtained at a helium pressure of 3 atm. with the e-beam gun located a distance of 7 cm from the afterglow chamber. For these parameters, the initial helium ion concentration should be

$$[+] \sim 5 \times 10^{14} \text{ cm}^{-3} \qquad \text{HPAC-1} \quad . \quad (15a)$$

Closer proximity to the e-beam gun was obtained with HPAC-1b and corresponded to an initial ion concentration at 3 atmospheres of

$$[+] \sim 1.7 \times 10^{15} \text{ cm}^{-3} \qquad \text{HPAC-1b} \quad (15b)$$

For purposes of the subsequent calculation of efficiencies, an expression for the input energy to the afterglow from the beam is useful. Considering the specified beam energy of 4.8 Joules and range of 450 cm/atm at the 60% power of 300 KeV, the average beam energy deposited in the plasma is

$$E_b = 7.8 \times [1 + 0.81\ell + 0.165\ell^2]^{-1} \quad \text{J/liter} \qquad . \qquad (16)$$

Better values for these parameters are contingent upon calibration of beam current and divergence, but it is believed that the interim use of these approximations is consonant with the current allocation of priorities in this project, as well as consistent with the accuracy at this stage of investigation of the data reported in the following section.

Several instructive problems were encountered with the initial operation of the system. Both RFI and X-ray noise were extreme and extensive protective measures were necessitated. Nested enclosures were constructed to suppress counting from the innermost, the RFI, X-rays, and RFI again. The innermost enclosure consisted of a copper bellows assembly bolted to the face of the e-gun and grounding through spring contact to the mounting ring supporting the foil window. Blocking the passage in the bellows was a .004" thick Mylar disk placed to protect the face of the e-gun from the possible back ejection of material from the foil window.

Surrounding the HPAC, together with the evacuation tube and valve to the dump chamber was a 1/16" lead enclosure with open ports to allow access to the optical windows and bellows connecting to the e-gun. Additional 0.5" lead plates were positioned in strategic locations to shadow the external instrumentation and operators.

The outermost, and most complete RFI shield consisted of 5 sides of a welded aluminum cube approximately one meter on a side. It can be lowered onto an aluminum base plate lying under the asbestos base of the bakeout oven.

Electrical contact between the case and base is assured by commercially available RFI gasketing. All gas inlets and vacuum lines through the base were grounded to base by sealing them to the base at the point of penetration with RFI gaskets. Contact between the penetrating tapered output end of the e-gun and the case is made with a sliding RFI gasket. The only unprotected openings through the enclosure are the two opposed circular ports centered on the same optical axis as the windows of the HPAC. Since there are no significant asymmetries or conductive penetrations through these holes, RFI radiated from them is at a minimum level and one which was found to be acceptable to the external instrumentation.

For the spectroscopic surveys of the spontaneous emission, three high-aperture systems have been found useful; an f/2 camera-spectrograph with about 300 Å/mm dispersion at the film plane, an f/4, 0.25 meter spectrometer with the exit slit removed to give about 100 Å resolution, and an f/4, 0.25 meter spectrograph coupled to a 4-stage image intensifier system arranged so that the dispersed spectrum of a single discharge could be photographed at a sensitivity where single-photon scintillations could be recorded.

The f/2-spectrograph was employed primarily to obtain the time-integrated spectra of the e-beam afterglow for the purpose of locating features of interest, as well as serving as an impurity monitor. Four pulses at the maximum beam energy were required for a useful exposure on Tri-X film developed to an ASA equivalent index of 2400.

The f/4-spectrograph/intensifier shown schematically in Figure 11 was to extend both sensitivity and resolution of the f/2 survey instrument. By adjustment of the accelerating voltage threshold sensitivity could be varied from the resolution of single photon scintillations to the integral of n successive photon scintillations within the decay time of the phosphor on the output screen.

Figure 11

Schematic representation of the spectrograph-image intensifier combination used to record spectra of single discharges at the level of sensitivity where single photon scintillations could be distinguished.

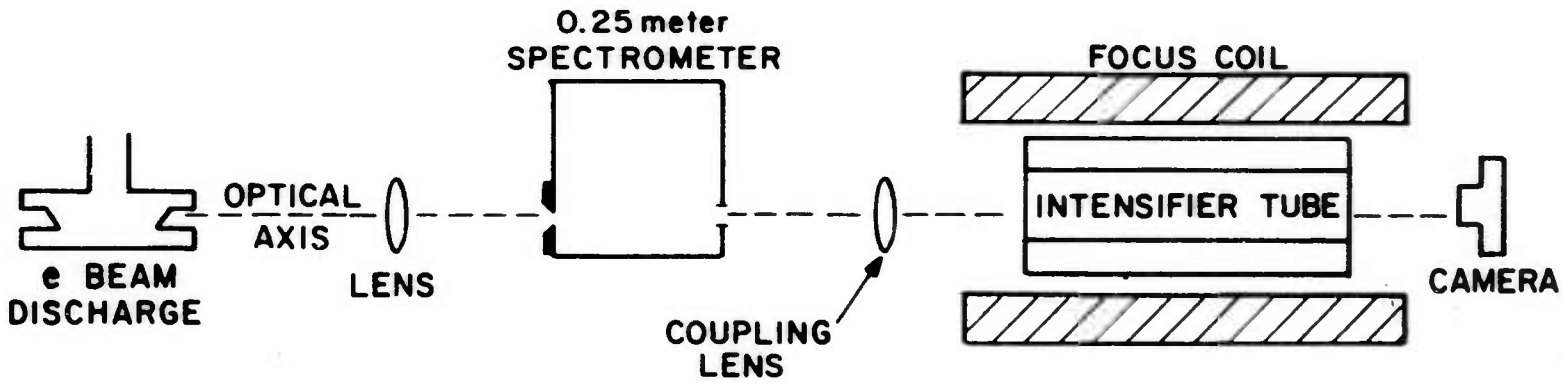
0.25 meter
SPECTROMETER
FOCUS COIL
OPTICAL
AXIS
INTENSIFIER TUBE
e BEAM
DISCHARGE
LENS
CAMERA
COUPLING
LENS

The 0.25 m spectrometer was used with a nine stage RCA-C31025C photomultiplier to obtain the transient intensity response for a particular 100 Å wavelength region. The useable region of sensitivity extended from 3000 Å to 8500 Å. The photomultiplier risetime of 1.5 nanosecond insured the transient intensity could be monitored with nanosecond resolution if adequate recording techniques were used. Intensities were such that typical signals were in the range of 0.1 to 1.0 volts into 50Ω with decay times in the range of a few x 10^{-8} sec. to a few x 10^{-7} sec.

This suggested the use of a Biomation 8100 transient recorder which provides the 8-bit digitization of input signals not less than 0.05 volts for full scale conversion over 2048 time increments of at least 10 nanoseconds each. The device was directly interfaced to the data acquisition computer currently serving the University's Atomic Physics group. Future refinements are under construction to give 300 psec resolution for at least the first 16 points.

Calibration of the 0.25 m spectrometer and detection system was accomplished by comparison to a standard of irradiance traceable to NBS. Detection sensitivities which calibrated the power at the spectrometer entrance slit to voltage at the 8100 input ranged from 20μ watts/volt at 4000 Å. The rather low sensitivity in the violet was primarily a consequence of the 6000 Å blaze wavelength of the grating, chosen to enhance the usually depressed red-sensitivity of most fast detection systems. A consideration of geometrical factors and volume sampled gave an overall calibration depending on wavelength which equated between one and two kilowatt/liter of incoherent power radiated from the e-beam afterglow to 1 volt of detected signal.

The addition to the system of an internal optical cavity contained in the HPAC-1b and having coincident optical axis with it has permitted the preliminary inference of optical gain from measurements of the enhancement of certain spectral features observed in the optical cavity. The cavity support-

ing these measurements is a sub-concentric geometry imposed by the availability of mirrors and the physical dimensions of the shielded system. The measurements discussed in the following section were obtained with multi-layer dielectric mirrors of maximum available reflectivity over the various 1000 Å regions examined.

A more quantitative system for the direct measurement of gain was constructed as shown in Figure 1[illegible]. Since the lifetimes for the source of molecular emissions ranged from 160 nsec. at 1 atmosphere to 26 nsec. at 7 atmospheres as discussed in Section II, it was necessary to use a rapidly pulsed light source for the measurement of small signal gain or absorption in a particular transition during the afterglow period. A nitrogen laser pumped, tunable dye laser with a FWHM of a few Angstroms was used in the differential path arrangement shown in Figure 12 to measure the attenuation or amplification of the beam reflected through the plasma by the internal dielectric mirror. Use of the optical delay line in the reference path allowed for the detection of both beams with a single photomultiplier and electronics system thus minimizing the drift of the balance of sensitivity between the paths. Resulting system stability was of the order of 6% with timing jitter between the e-beam and the dye laser being of the order of a recombination lifetime. However, as accuracy of the timing measurement was around 4 nsec., adequate resolution of the particular phase of the afterglow sampled by the dye laser beam could be established.

The success in the use of this system in the preliminary measurements at 6400 Å discussed in the following section indicates it will be the primary technique utilized in the measurement of gain at the other wavelengths of importance in the helium afterglow. The dye laser technology is well enough developed to support investigation over the 3500 Å - 7500 Å spectral region

Figure 12

Experimental system for the direct measurement of time-resolved gain spectra.

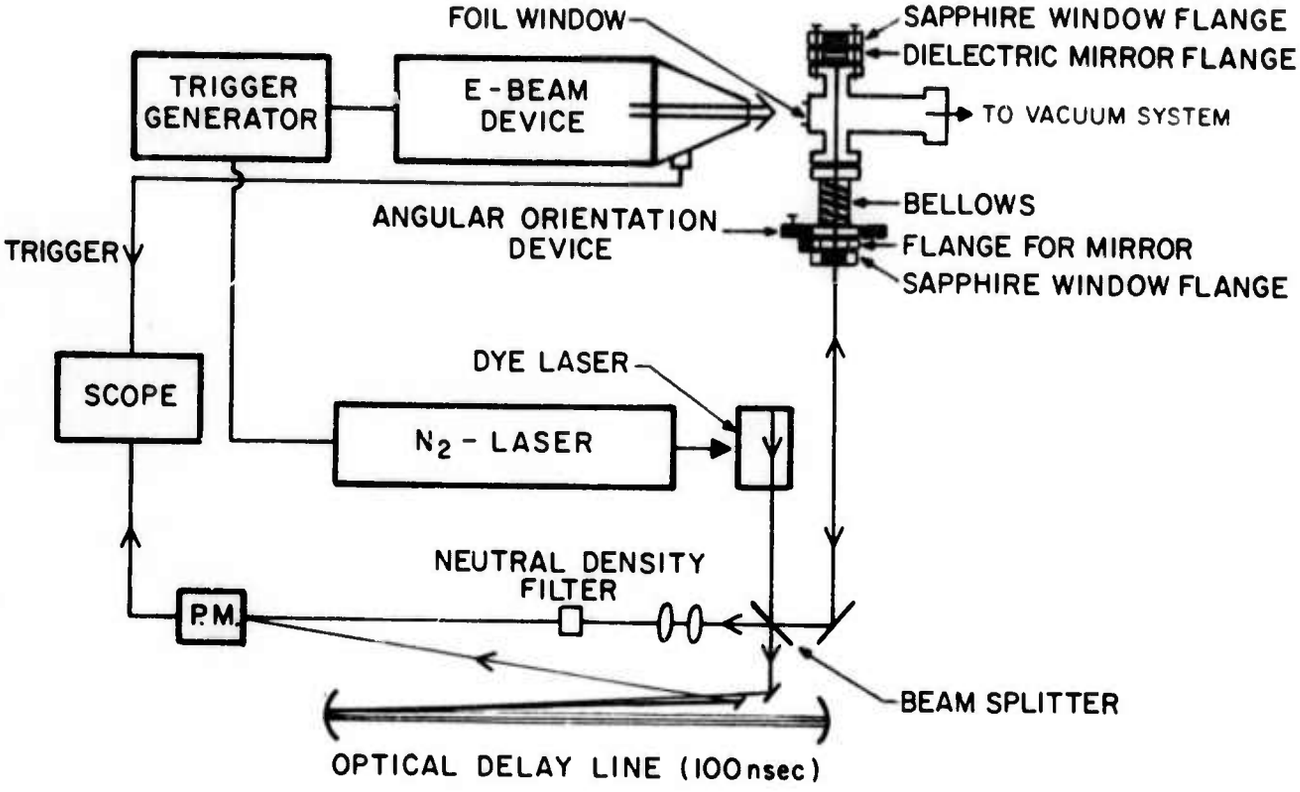
FOIL WINDOW
SAPPHIRE WINDOW FLANGE
DIELECTRIC MIRROR FLANGE
TRIGGER GENERATOR
E-BEAM DEVICE
TO VACUUM SYSTEM
BELLOWS
ANGULAR ORIENTATION DEVICE
TRIGGER
FLANGE FOR MIRROR
SAPPHIRE WINDOW FLANGE
DYE LASER
SCOPE
N_2 - LASER
NEUTRAL DENSITY FILTER
P.M.
BEAM SPLITTER
OPTICAL DELAY LINE (100nsec)

and efforts are currently underway to improve synchronization between the N_2-laser pumping source and the e-beam gun. It is expected these developments will permit the controlled sampling of the various afterglow phases with synchronization comparable to a fraction of a recombination lifetime.

IV. TECHNICAL RESULTS

Preliminary values were obtained for the most important diagnostic parameters characterizing the e-beam afterglow excited in 3 atmospheres of helium with the previously described HPAC-1 system.[1] Confirmation and extension[2,15] of these values to cover the one to five atmosphere pressure range was accomplished in the HPAC-1b chamber at greatly improved gas purity. A preprint of the resulting article submitted to Physics Letters appears in Appendix I. Parameters considered to date in this work are a) output wavelengths, b) spontaneous emission, energies and peak power levels, c) incoherent output efficiencies, d) inferred optical gains, e) stimulated emission, and f) stimulated output efficiencies. Each is considered in the following subsections, and those reported previously are reviewed to the extent that they clarify present results.

a) Output wavelengths

Figure 13 presents a survey spectrum of the spontaneous emission from a single discharge in the HPAC-1b system made with the f/4 spectrograph-image intensifier combination having greatly improved sensitivity and resolution over conventional spectrographic systems. Principal limitation on both quantities have been reduced to the quantum noise imposed by the discrete nature of the photodetection events. All the information available in the spectrum has been recorded. Primary detection occurs with an S-11 photocathode with subsequent acceleration and multiplication of the emitted photoelectrons. In contrast to direct film recordings[1,2], this system has an enhanced sensitivity in the shorter wavelength region and a pronounced cut-off in the red around 6400 Å.

Relative sensitivity of the intensifier tube as a function of wavelength is shown in Figure 14.

Figure 13

Survey spectrum of the visible region made with the f/4 spectograph - image intensifier system. Long wavelengths are to the left. Each spectrum is a time-integrated record of the afterglow from a single discharge of the e-beam gun in helium at 3 atmospheres in the HPAC-1b system. Exposures are for different accelerating voltages corresponding to different values of the number of superimposed photon scintillations required within the decay time of the output phosphor to reach the threshold for photographic detection. From top to bottom, accelerating voltages are 25, 30, 35 and 40 KV, the last two satisfying the requirements for the detection of scintillations from single photoelectrons.

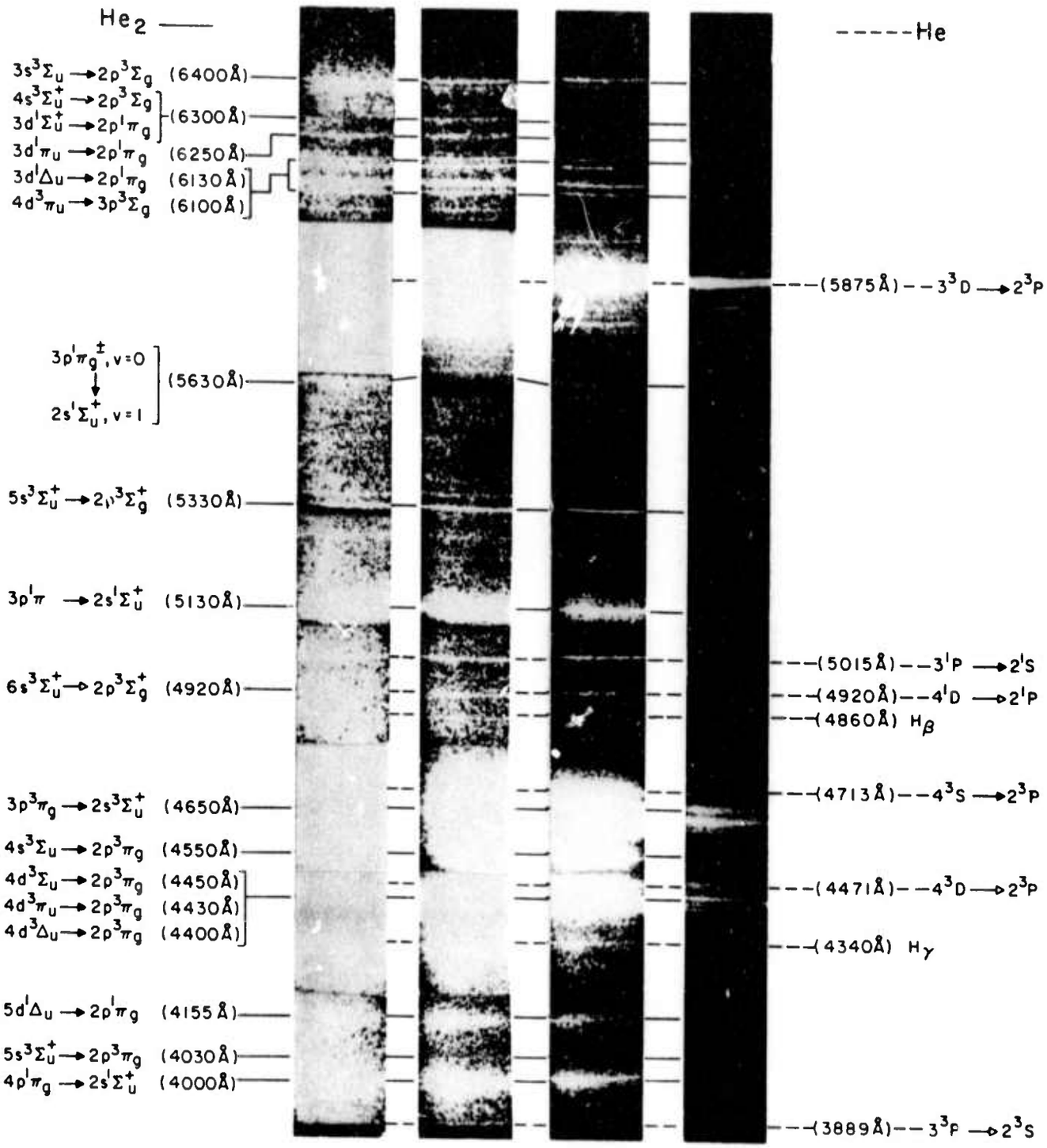
He2
He
$3s^3\Sigma_u \rightarrow 2p^3\Sigma_g$ (6400Å)
$4s^3\Sigma_u^+ \rightarrow 2p^3\Sigma_g$
$3d^1\Sigma_u^+ \rightarrow 2p^1\pi_g$ (6300Å)
$3d^1\pi_u \rightarrow 2p^1\pi_g$ (6250Å)
$3d^1\Delta_u \rightarrow 2p^1\pi_g$ (6130Å)
$4d^3\pi_u \rightarrow 3p^3\Sigma_g$ (6100Å)
$3p^1\pi_g^{\pm}, v=0 \rightarrow 2s^1\Sigma_u^+, v=1$ (5630Å)
$5s^3\Sigma_u^+ \rightarrow 2_{1,}{}^3\Sigma_g^+$ (5330Å)
$3p^1\pi \rightarrow 2s^1\Sigma_u^+$ (5130Å)
$6s^3\Sigma_u^+ \rightarrow 2p^3\Sigma_g^+$ (4920Å)
$3p^3\pi_g \rightarrow 2s^3\Sigma_u^+$ (4650Å)
$4s^3\Sigma_u \rightarrow 2p^3\pi_g$ (4550Å)
$4d^3\Sigma_u \rightarrow 2p^3\pi_g$ (4450Å)
$4d^3\pi_u \rightarrow 2p^3\pi_g$ (4430Å)
$4d^3\Delta_u \rightarrow 2p^3\pi_g$ (4400Å)
$5d^1\Delta_u \rightarrow 2p^1\pi_g$ (4155Å)
$5s^3\Sigma_u^+ \rightarrow 2p^3\pi_g$ (4030Å)
$4p^1\pi_g \rightarrow 2s^1\Sigma_u^+$ (4000Å)
(5875Å) $3^3D \rightarrow 2^3P$
(5015Å) $3^1P \rightarrow 2^1S$
(4920Å) $4^1D \rightarrow 2^1P$
(4860Å) H_β
(4713Å) $4^3S \rightarrow 2^3P$
(4471Å) $4^3D \rightarrow 2^3P$
(4340Å) H_γ
(3889Å) $3^3P \rightarrow 2^3S$

Figure 14

Graph as a function of wavelength of the relative sensitivity of the image intensifier system used to obtain the data of Figure 13.

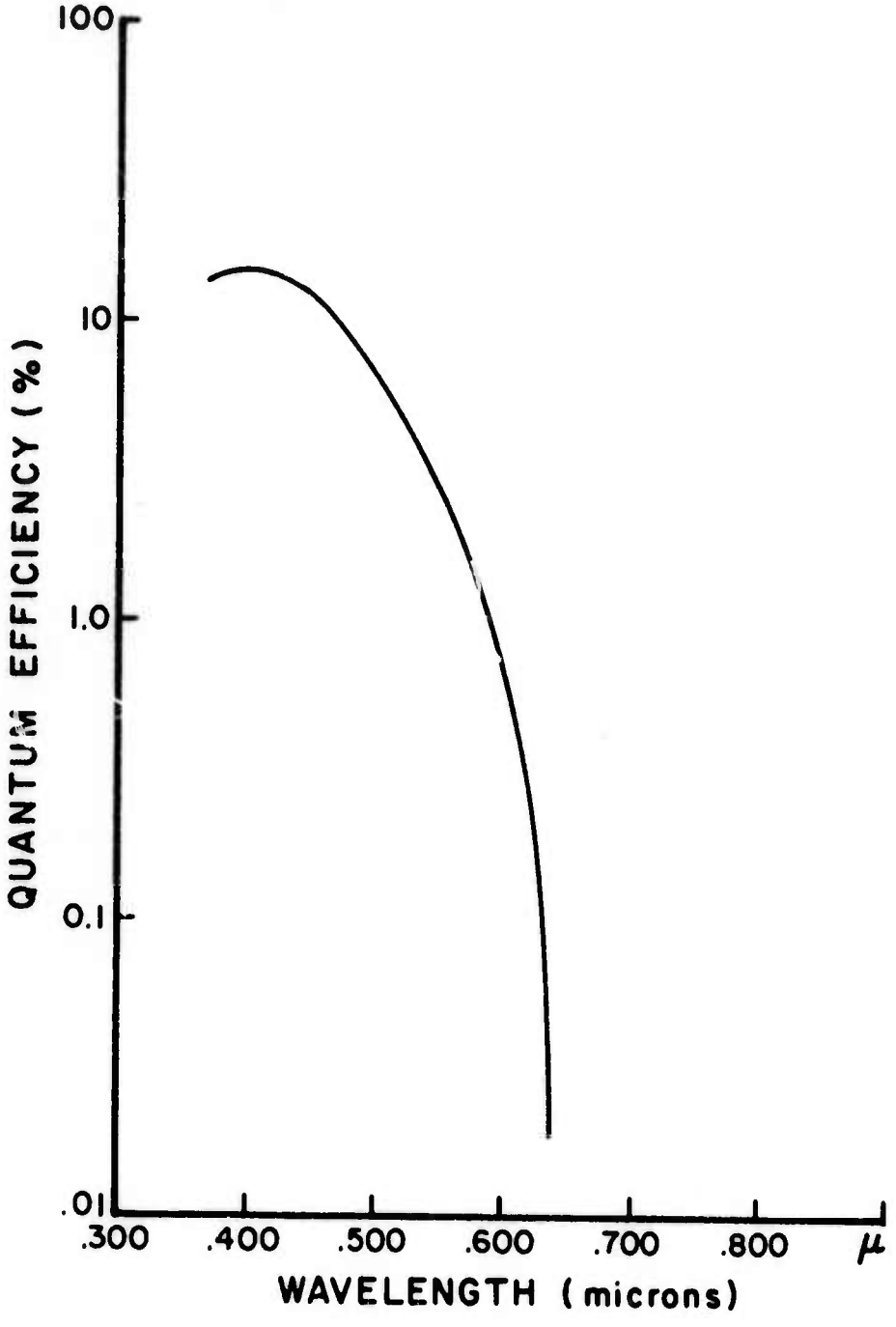
100
10
1.0
0.1
.01
QUANTUM EFFICIENCY (%)
.300
.400
.500
.600
.700
.800
μ
WAVELENGTH (microns)

Several exposures of the spectrum are shown in Figure 13 and correspond to different values of accelerating voltage on the image intensifier tube and, hence, to different values of gain for the photoelectron amplification. Each represents a different value of the number of successively superimposed photon scintillations required within the decay time of the output phosphor to reach the threshold exposure of the recording film. From top to bottom, the exposures represent increasing accelerating voltage with the last two strips satisfying the requirements for the detection of scintillations from single photoelectons. Values of actual photoelectron gain corresponding to the accelerating voltages shown can be read from Figure 15.

In Figure 13, most of the He_2 spectrum is seen, with principal interest being directed toward the relatively enhanced features in the red. However, it can be seen that the other members of the "favorable" Rydberg-series discussed in the introductory material are present. In particular

1. the $ms^3\Sigma_u^+ \rightarrow 2p^3\Pi g$ series convergent at 3680 Å is represented strongly by the m=3,4 and 5 members at 6400 Å, 4540 Å and 4030 Å, respectively, and
2. the $mp^1\Pi g \rightarrow 2s^1\Sigma_u$ convergent at 3130 Å and terminating on a state optically connected to the $1s\sigma^2 2s\sigma$ repulsive ground state is evidenced by the relatively strong m=3 and 4 components at 5130 Å and 4000 Å, respectively. This latter series is of tangential interest in that, if lasing could be accomplished for one component, the delivery of population to the $2s^1\Sigma_u$ state might occur at a rate sufficient to invert the vacuum - UV transition from this state to the repulsive ground state.

The spectral information of Figure 13 is summarized in Figures 16 and 17 which are energy level diagrams of

Figure 15

A graph of photoelectron gain as a function of accelerating voltage for the image intensifier system used to record the spectra of Figure 13.

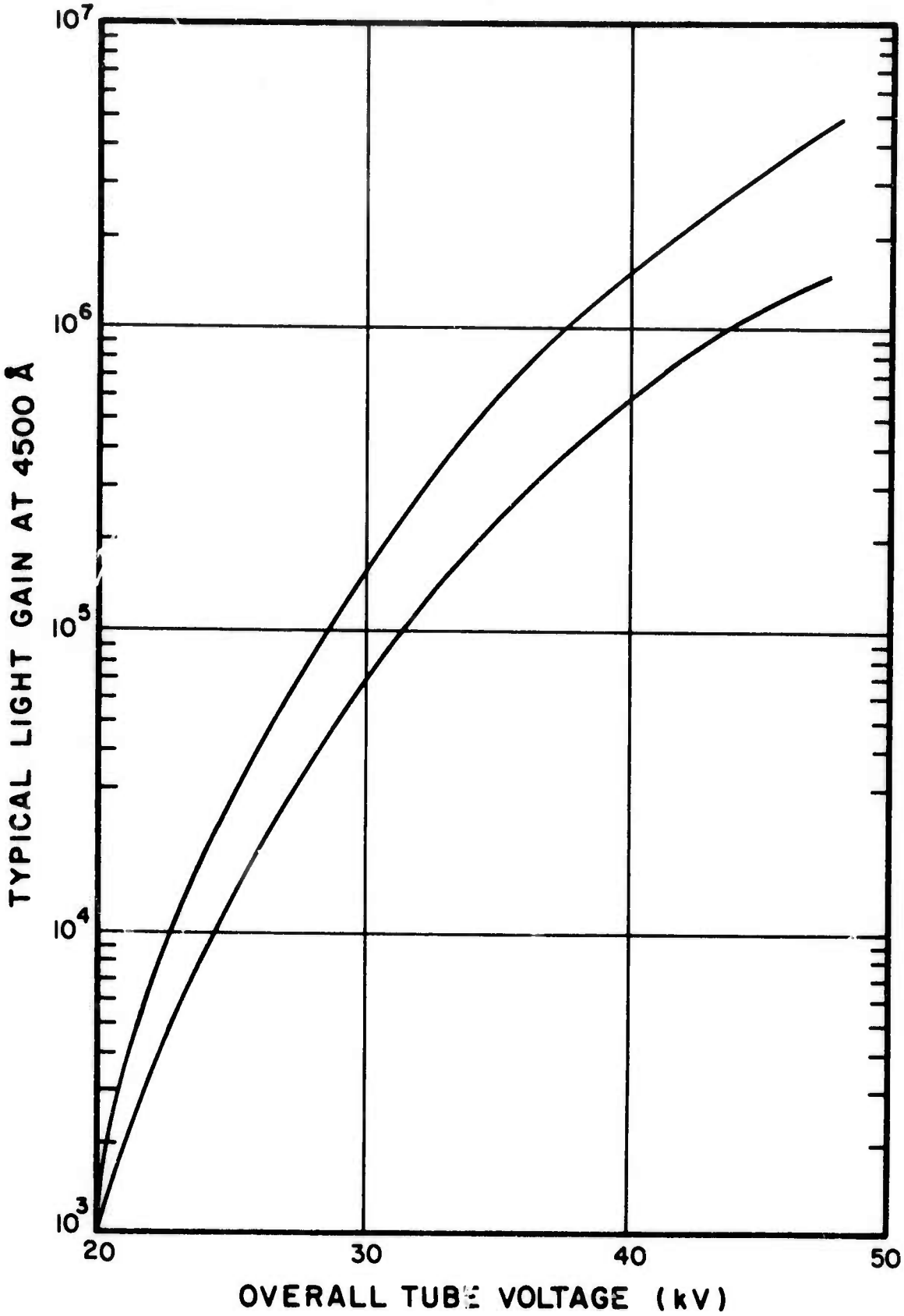
10^7
10^6
10^5
10^4
10^3
TYPICAL LIGHT GAIN AT 4500 Å
20
30
40
50
OVERALL TUBE VOLTAGE (kV)

Figure 16

Energy level diagram of atomic helium showing for clarity only those states participating in transitions observed with appreciable intensity in the afterglow at three atmospheres.

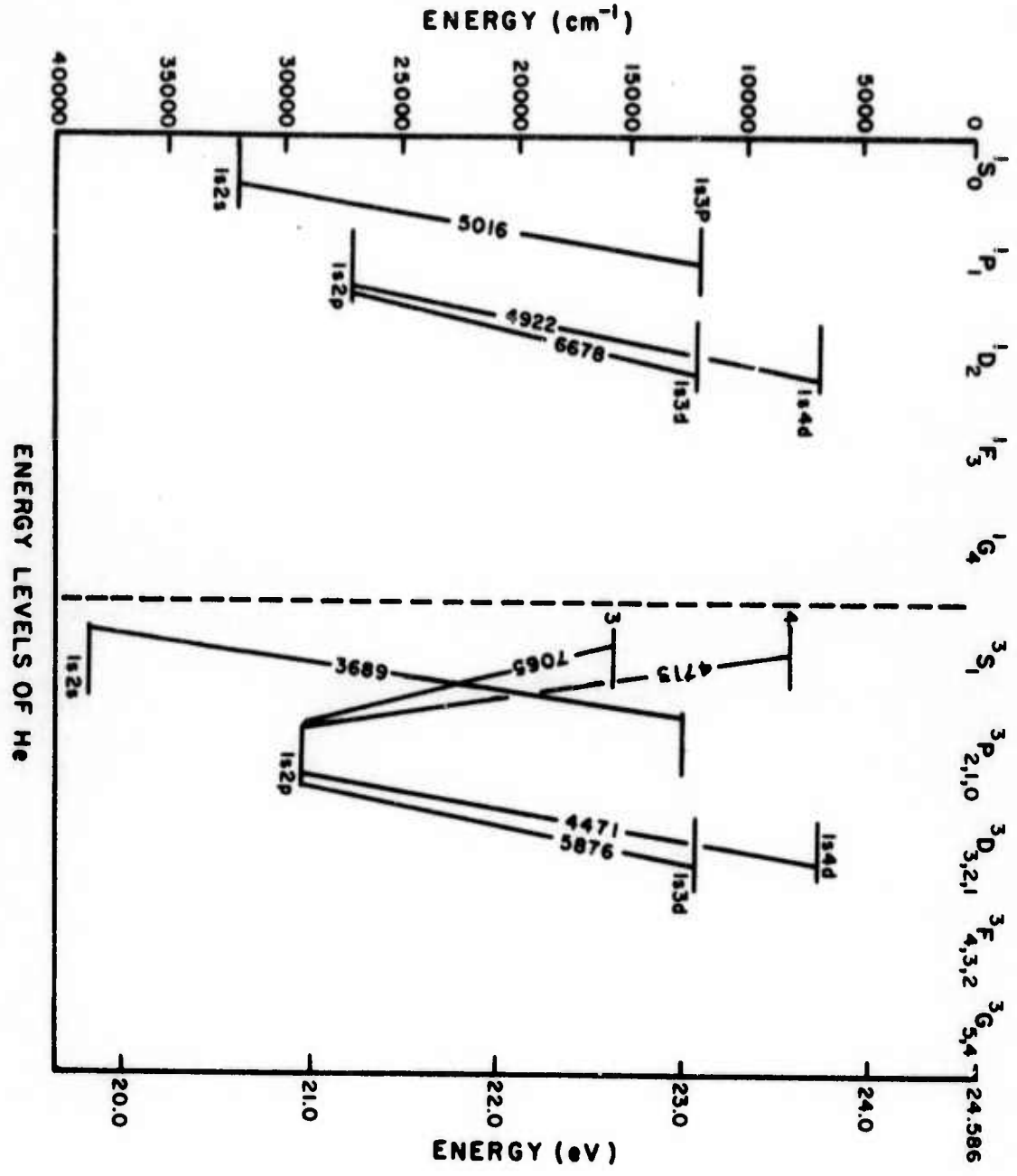
ENERGY (cm⁻¹)
40000
35000
30000
25000
20000
15000
10000
5000
0
ENERGY LEVELS OF He
1s2s
1s3P
5016
1s2p
4922
6678
1s3d
1s4d
1S0
1P1
1D2
1F3
1G4
3
4
3689
7065
4713
1s2s
1s2p
4471
5876
1s3d
1s4d
3S1
3P2,1,0
3D3,2,1
3F4,3,2
3G5,4
20.0
21.0
22.0
23.0
24.0
24.586
ENERGY (eV)

Figure 17

Energy level diagram of molecular helium showing for clarity only those states participating in transitions observed with appreciable intensity in the afterglow at three atmospheres.

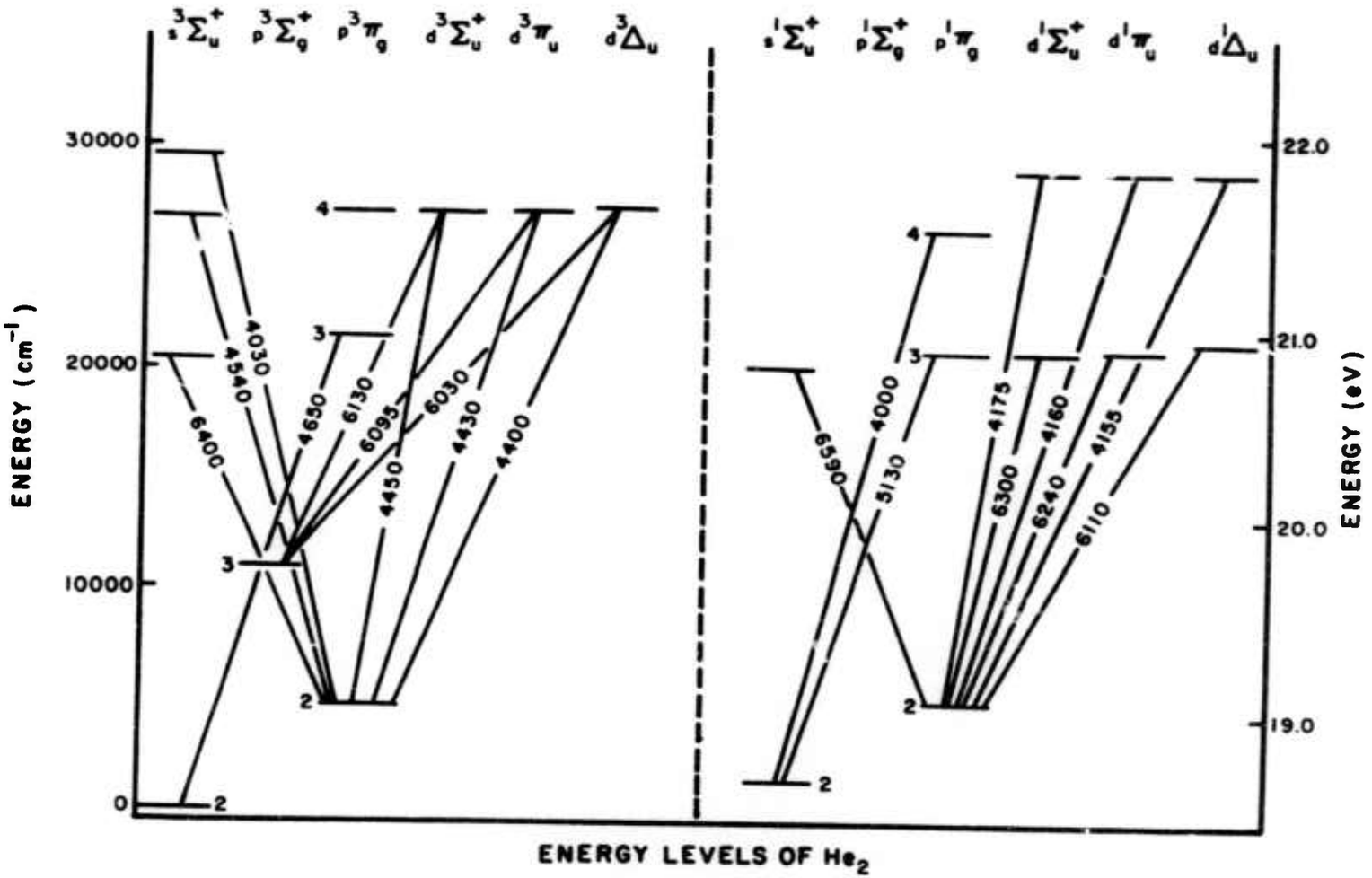

ENERGY LEVELS OF He_2

He and He_2 in which for clarity only those states participating in transitions observed in the afterglow with appreciable intensity are shown. The general observation can be made that the abundance of He_2 levels excited is characteristic of a collisional-radiative recombination origin of the light with good collisional mixing between levels.

The bands generally appear at relative intensities which could be reasonably expected from radiative and collisional cascading in the course of the stabilization of the collisional-radiative recombination of He_2^+. This is the cascading discussed in Section II. Of course, such comparisons are quite qualitative and dependent upon subjective averaging over a considerable variety of low pressure helium recombination spectra. In addition, the following transitions appear anomalously enhanced:

1. the $3s^3\Sigma_u^+ \rightarrow 2p^3\Sigma_g$ at 6400 Å
2. the transitions from the 4d complex to the pσ level at 6130 and 6100 Å.

These represent transitions which, in a sense, compete with the normally intense 3-d complex. As can be seen from Figure 17, the third is equivalent to a short-circuit from principal quantum level 4 to 2 by passing the "normal" stabilization current which tends to relax captured electrons from one principal quantum level at a step. The first can be rationalized as a transition from a state benefitting from one of the "fine-tuning" effects of collisional stabilization which tend to move bound electron populations back and forth between angular momentum sub-levels corresponding to the same principal quantum number. It is this effect which, as discussed in Section II, would allow a lasing transition to capture virtually all of the stabilizing electron current between principal quantum levels. In the case of

the 6400 Å transition, the particular radiating sublevel lies at a somewhat lower energy, ∿ 0.22eV, than the d-complex and should show a gain of population relative to the d-complex when the electron density is high and such "lateral" collisions are frequent.

The rather restricted excitation of the He spectrum is, conversely, more characteristic of some type of selective excitation and warrants further investigation of the possible kinetic processes which might supply such upper state excitation.

b) Spontaneous emission, energies and peak power levels

Each of the spectral features in the wavelength range of the instrumentation showed one or a combination of three basic transient responses, each correlating with a different excitation mechanism as shown in Figure 18.

A typical example of an emission showing a combination of direct e-beam, and recombination excitation is found in the data of Figure 19. In this figure, the emission of the $3^3S \rightarrow 2^3P$ line of atomic helium at 7065 Å is recorded on a horizontal scale of 200 nanoseconds/division by 81 watts/liter per division vertically. While the upper 3^3S state of this transition is optically forbidden to the ground 1^1S state and hence an unlikely candidate for excitation by the primary electrons, it does have a non-zero cross section for secondary electrons which might be expected to have energies near the threshold for excitation of this system. Most probably the situation here is analogous to the excitation of the N_2 C-state in the e-beam N_2 laser. That state is also optically forbidden to the ground X-state and as a consequence is only weakly excited by the higher energy primary electrons but strongly excited by the secondary electrons whose energy lies only slightly above the excitation threshold.

Detailed examination on an expanded time base of the leading edges of the molecular emission as typified by the one at 6400 Å showed no evidence of a component of e-beam excitation either by primary or secondary electrons ac

Figure 18

Time evolution of selected atomic and molecular emissions at 3 atmospheres illustrating the three basic excitation mechanisms observed: 1) 5015 Å atomic transition, direct excitation by primary electrons, 2) 7065 Å atomic transition, excitation by energetic secondary electrons and 3) 6400 Å molecular transition, excitation by recombination of He_2^+ ions and cool secondary electrons.

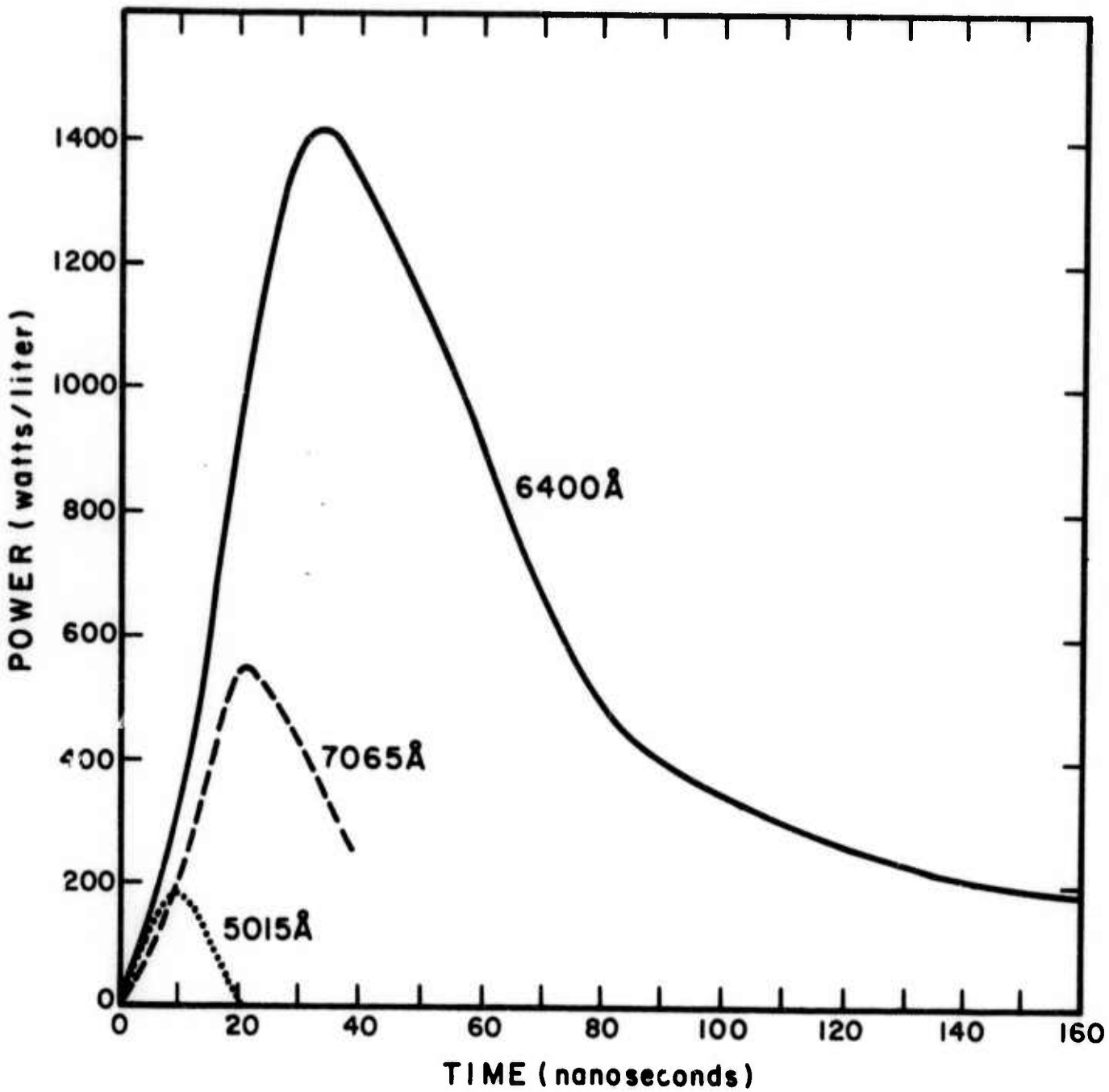
POWER (watts/liter)
1400
1200
1000
800
600
400
200
0
6400Å
7065Å
5015Å
0
20
40
60
80
100
120
140
160
TIME (nanoseconds)

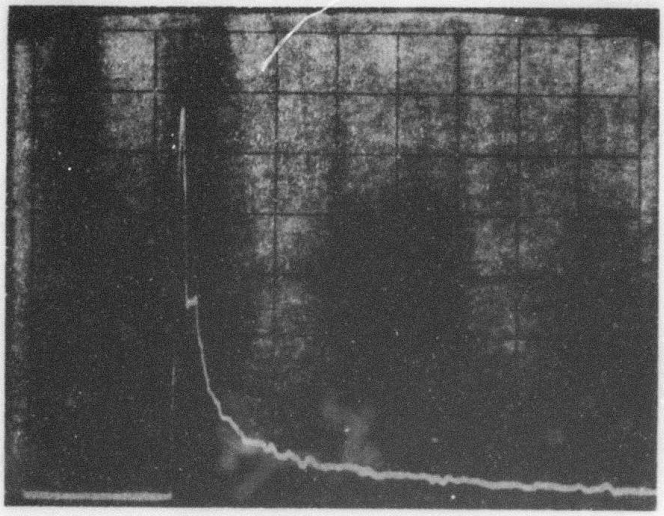

Figure 19: Time evolution of a single pulsed excitation of the 7065Å line which shows both an early component due to excitation from energetic secondary electrons and a later recombination component. Scales are 200 nanoseconds per horizontal division and 81 watts/liter per vertical division.

would be expected from the absence of a stable He_2 ground state. Rather, the leading edge shows a rise time consistent with the decay of the component of the 7065 Å excitation inferred to be due to the secondary electrons. This also is consistent with a simple model which requires the secondary electrons to cool before they can participate in collisional recombination with the ions. If they are energetic enough to excite the 7065 Å line, they are too hot as a group to recombine with the He_2^+ ions to give the 6400 Å radiation.

From these considerations an interesting comparision can be made of the output energies resulting from each process. These are summarized in Table IV.

Table IV

Comparison of Measured Output Energies

from Direct Excitation and Recombination

at 3 Atmospheres

Line	Direct e-beam Excitation (micro-Joules/liter)	Recombination (micro-Joules/liter)
5015 Å	$\sim$ 1.8	-
7065 Å	$\sim$ 16	71
6400 Å	$<$ 2.7	110

Table IV serves to underscore the comments made in Section II that the potential for recovering much of the e-beam energy "lost" to ionization is quite high in recombination systems.

Implicit in the development of data of the sort presented in Table IV is a knowledge of lifetimes by which the peak powers are multiplied to estimate the output energy per pulse. The particular lifetimes desired are

the lifetimes against recombination defined by equation (7), Section II, and tabulated in Table III. The energy output, E, can be written in terms of these quantities as

$$E = \int_0^\infty I(t)dt \quad , \qquad (17)$$

which becomes upon substitution from (10)

$$E = \int \{I_{(0)}^{-\frac{1+\eta}{2+\eta}} + K(1+\eta)(CK)^{-\frac{1+\eta}{2+\eta}} t\}^{\frac{2+\eta}{1+\eta}} dt \quad . \qquad (18)$$

Upon integration followed by substitution from (12) and (11), this becomes

$$E = I(0)\tau_0 \quad . \qquad (19)$$

Table V summarizes the resulting energies per pulse radiated spontaneously.

Table V

Summary of the Energies per Pulse of the Principal Spectral Features Emitted Spontaneously

Wavelength	Energy (micro-Joules/liter)			
Pressure (atm.)	1	3	4.2	7
$\underline{He_2}$				
6400 Å	104	52.5	35.0	32*
4650 Å	42.5	31.4	25.2	24*
$\underline{He}$				
7065 Å	-	54*	59*	92*
6678 Å	38.6*	24.2	12.1*	15.0*
5875 Å	665	905	2200	4400*

*HPAC-2

c) Incoherent Output Efficiencies--From the data of Table V and the input e-beam energy estimated in equation (16), the output efficiency can be obtained for the prominent spectral features examined. Table VI summarizes these results.

Table VI

Efficiencies for the Incoherent Radiation Observed from the Recombination

Wavelength	Efficiency		
Pressure (atm)	1	3	4.2
He_2			
6400 Å	.0057%	.00096%	.00054%
4650 Å	.0023%	.00057%	.00032%
He			
7065 Å	--	.001%	.001%
6678 Å	.002%	.0004%	.00015%
5875 Å	.036%	.016%	.028%

Efficiencies are not particularly impressive but this is not surprising because in the absence of a stimulated transition, at these electron desnities a large fraction of the level to level stabilization should be accomplished by non-radiative transitions. According to theory, if a stimulated transition can be developed, the energy now lost to the collisional channels could be tapped by a competing radiative transition, if strongly induced. This effect is illustrated in part f) of this section for the case of the 6400 Å band.

d) Inferred Optical Gains--The gain or loss of selected transitions was inferred over the widest range of wavelengths from the measurement of the relative enhancement of the feature observed in a resonant optical-cavity. Two experimental arrangements were employed as shown in Figures 20(a) and 20(b). In each case, the "back" mirror, farthest from the recording camera was a multilayer dielectric mirror, 15 mm in diameter and totally reflecting, r>99.5%

Figure 20

Schematic representations of the two optical arrangements used in the enhanced brightness measurements referenced in Section III. In each case, the "back" mirror was totally reflecting, r>99.5% over the 5800 Å to 6800 Å region while the front mirror reflected ∿ 97% of the light in the 4400 Å to 7000 Å interval.

(a) The rear mirror and radiation from the interposed plasma was viewed and photographed along the low-loss axis of the resonant cavity.

(b) The image formed at the film plane in (a) was magnified and projected onto the input photocathode of the image intensifier. Image intensity lost in the magnification was recovered by amplification in the image intensifier. The image on the output flourescent screen of the intensifier was then photographed.

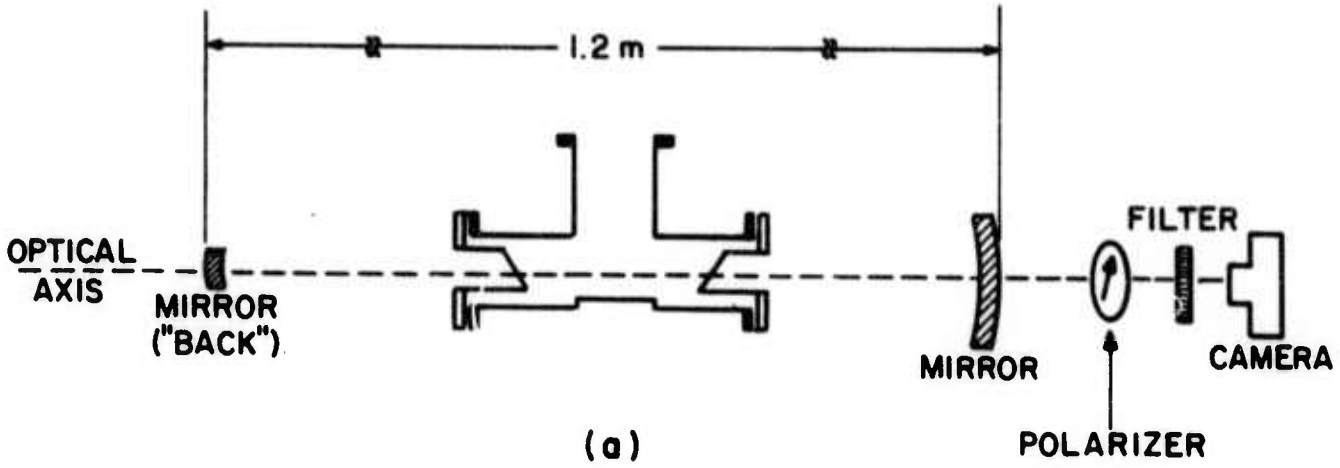
1.2 m
OPTICAL AXIS
MIRROR ("BACK")
FILTER
MIRROR
CAMERA
POLARIZER

(a)

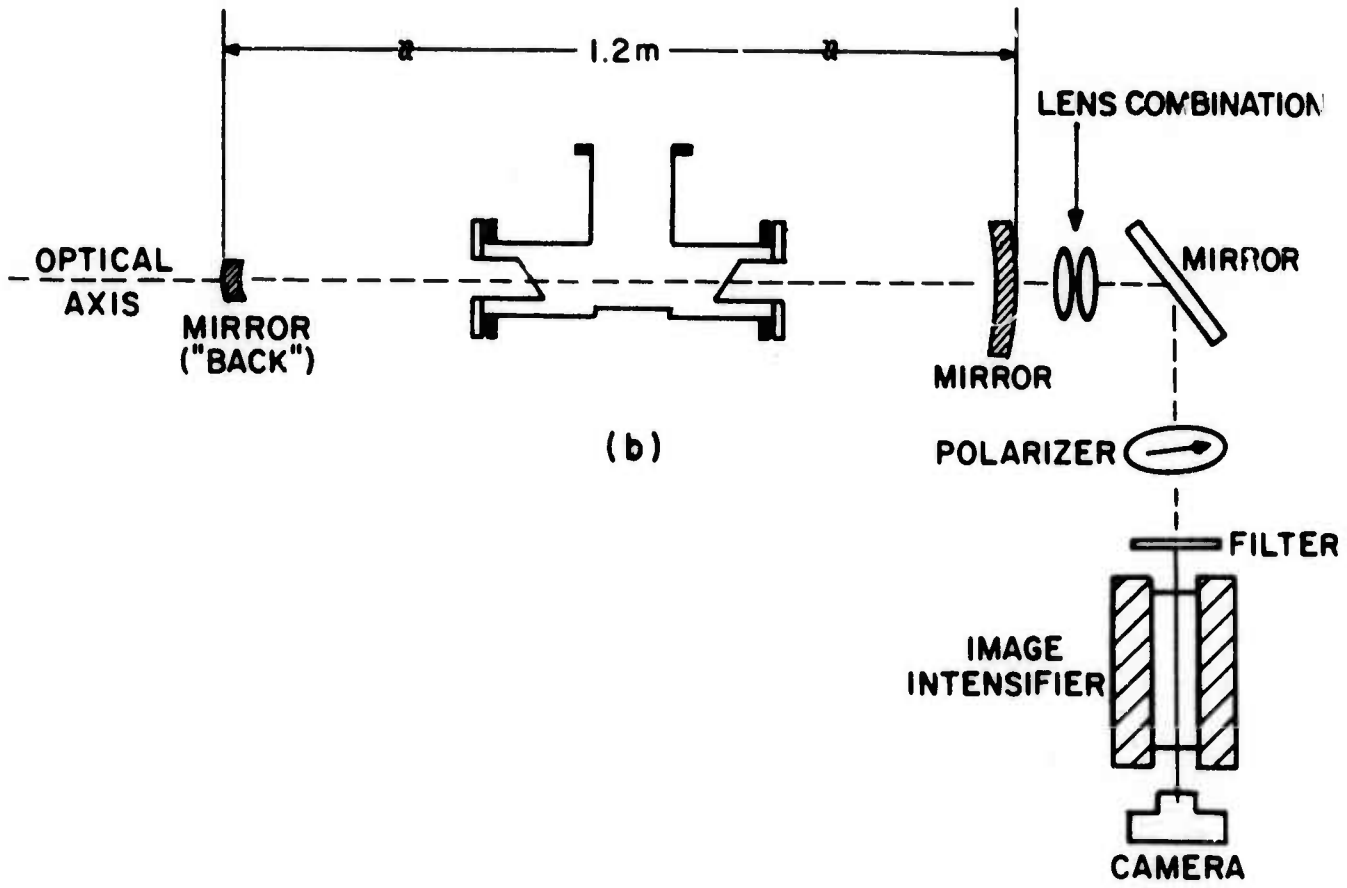
1.2 m
LENS COMBINATION
OPTICAL AXIS
MIRROR ("BACK")
MIRROR
MIRROR
POLARIZER
FILTER
IMAGE INTENSIFIER
CAMERA

(b)

over the appropriate wavelength region. The "front" mirror was a wide band dielectric mirror reflecting ∿ 97% of the light over the 4400 Å - 7000 Å region. It was 25 mm in diameter and in the case of the arrangement shown in Figure 20 (a) formed the limiting aperture of the recording system.

In such a configuration, the apparent axial brightness of an optically active plasma has been predicted[16] to depend upon experimental parameters as shown in Figure 21 for stable geometries lying between the confocal and the concentric.

Plotted are F values where

$$F=G(M-1) \quad , \qquad (20)$$

M is the ratio of apparent brightness of the plasma interposed between the point of observation and the "back" mirror to the brightness viewed from the same axial point in the absence of the back mirror, ie., purely incoherent radiation, and G is a scale factor depending only upon cavity geometry and difficult to compute precisely. Curves are shown as functions of loss coefficient per transit of the plasma and parameterically as functions of a_o, the passive optical transmissivity of the cavity and afterglow container per roundtrip. For the experiments reported here, the unloaded cavity had a transmissivity of $a_o \sim 0.85$, equivalent to a loss per roundtrip of 15% for the low-loss polarization corresponding to the Brewster angle. Since the emission sampled is principally incoherent, the intensity from the low-loss polarization cannot be selected uniquely by an external polarizer. A sum of that intensity, together with the projections of intensity components from the higher loss polarizations onto the low-loss axis is obtained when the angle of the analyzing polarizer corresponds to that axis. In this sense, the use of a single curve from Figure 21 can only be considered an approximation.

While this together with the uncertainties in calibrating the geometric scale factor, G, make equivocal the quantitative interpretation of the data

Figure 21

Plot of the calculated F-factors for enhancement from equation (1) as a function of fractional loss (+) or gain (-) coefficient per transit of the plasma. Values of the passive optical transmissivity, a_o, for the cavity and afterglow container were varied parametrically as indicated.

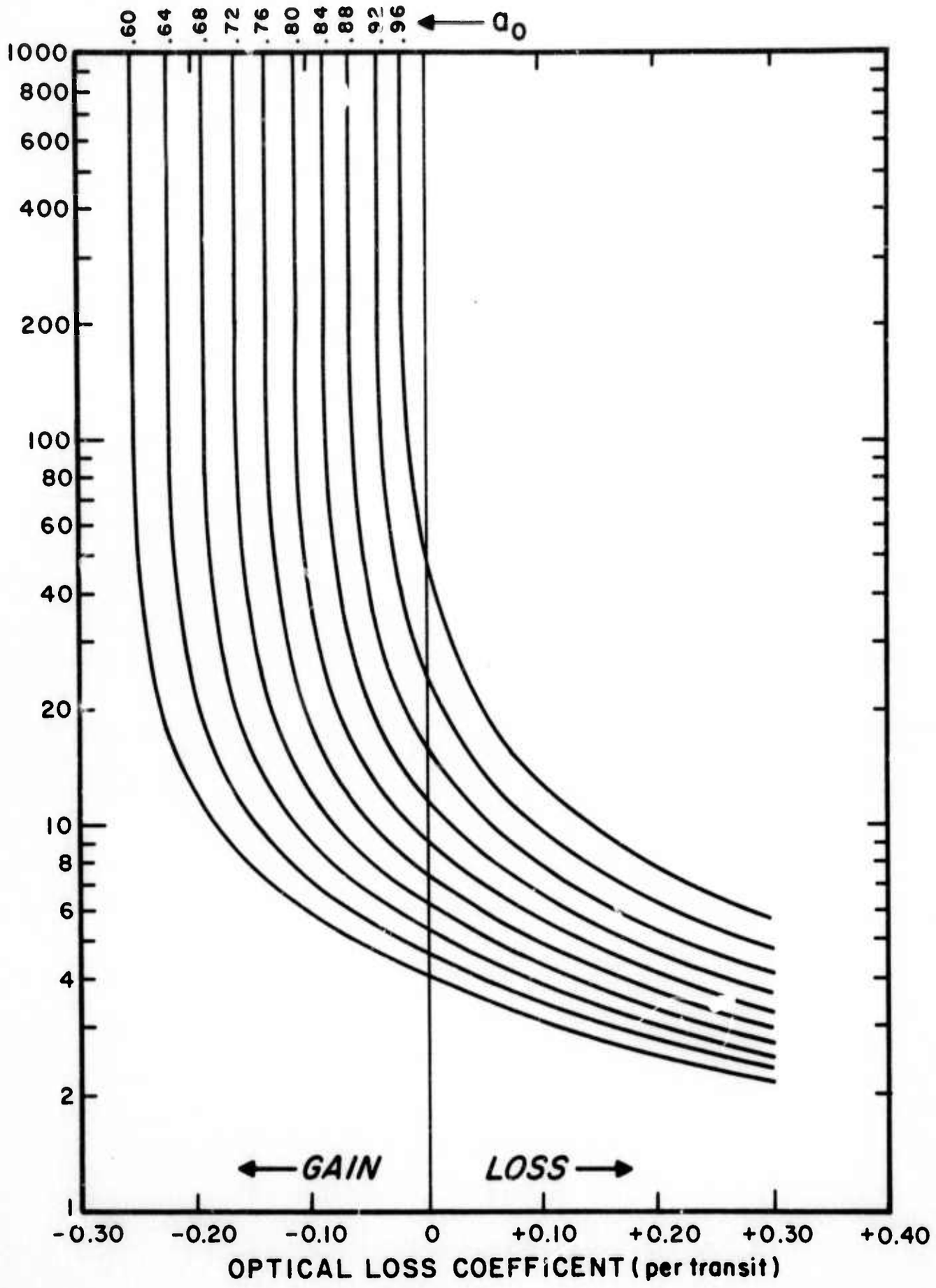
.60
.64
.68
.72
.76
.80
.84
.88
.92
.96
a_0
1000
800
600
400
200
100
80
60
40
20
10
8
6
4
2
1
GAIN
LOSS
-0.30
-0.20
-0.10
0
+0.10
+0.20
+0.30
+0.40
OPTICAL LOSS COEFFICENT (per transit)

collected, from the viewpoint of this presentation, the most important feature of Figure 21 is simply the general form of the curves. As would be expected, near the threshold for lasing the decreasing enhancement of apparent brightness caused by the back mirror should be strongly and non-linearly dependent upon loading of the cavity with successive increments of passive loss. This forms the basis of the measurements presented below.

Figures 22 show the enhanced brightness recorded by light unselected for polarization, but filtered to retain principally the 5875 Å component. Figure 22(a) shows the appearance of the rear mirror and interposed plasma and (b) shows only the plasma, the rear mirror having been covered with a mechanical shutter. As would be expected, higher contrast is obtained if an analyzing polarizer is used to select the intensity components projected along the axis corresponding to the lowest loss mode of the cavity as determined by the Brewster angle windows.

With a geometric factor estimated to be of the order of 5, the gain indicated is sufficiently large to suggest proximity to the lasing threshold. As mentioned above, this implies a high sensitivity to cavity loading and provides the basis for a significant test of gain. By loading the cavity with successive increments of passive loss, a strongly non-linear dependence of decreasing enhancement should be observed. Figures 23 (a), (b), (c) and (d) present the enhancements observed for the low-loss polarizations for the cavity with, respectively, interposed 0, 8, 16 and 24%, increments of passive loss. It can be seen that it is the first increment which causes the most significant decrease in intensity with subsequent additions causing little or no visible changes. Calibration against a density wedge shows that the first increment causes a reduction of enhancement by a factor of 2.5.

Although quantitative interpretation is impeded by the transient nature of the amplifying medium, the qualitative effect of the sensitivity of the

Figures 22

Photographs of the enhanced brightness of the afterglow light from the region of the plasma lying in the resonant cavity and observed along its axis with experimental configuration shown in Figure 20(a). The light was not selected with respect to polarization, but filtered to retain principally the 5875 Å component.

(a) Photograph showing the rear mirror and radiation from the interposed plasma

(b) Photograph showing the apparent brightness of the incoherent emission from the plasma viewed as in (a), but with the rear mirror covered.

All polarization modes sampled
"Back" mirror uncovered.

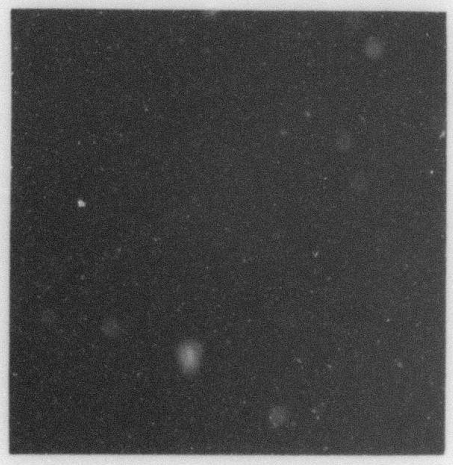

All polarization modes sampled
"Back" mirror covered.

Figures 23

Photographs supporting the investigation of the sensitivity of brightness enhancement ratios to loading of the resonant cavity. For these photographs, the analyzing polarizer was oriented to pass intensity components corresponding to the lowest loss mode of the optical cavity and the light filtered to select principally the 5875 Å wavelength. The series shows the effect of loading the cavity with successive 8% increments of interposed passive loss.

(a) 0% passive loss increment

(b) 8% passive loss increment

(c) 16% passive loss increment

(d) 24% passive loss increment

0% passive loss increment.

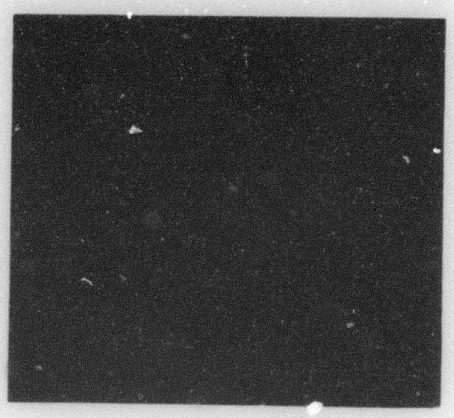

8% passive loss increment.

16% passive loss increment.

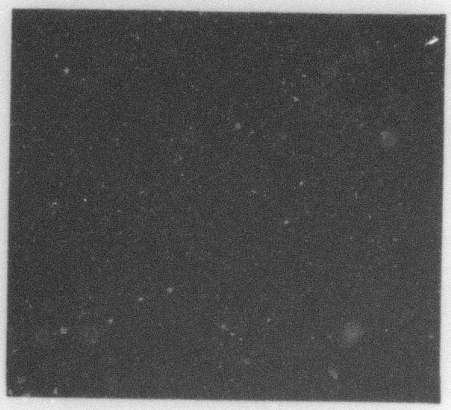

24% passive loss increment.

enhanced output to cavity loading served as a useful list to identify spectral features having the potential for stimulated emission. In this way, the bands at 6400 Å, 5130 Å, and 4400 Å, as well as the atomic line at 5875 Å, were identified as promising. The detailed investigation of the first is reported in the following material.

e) Stimulated Emission--The ability of the helium afterglow to sustain stimulated emission was investigated with the dye laser apparatus of Figure 12. By directly measuring the attenuation or amplification of the probing beam, the coefficient of loss or gain could be directly determined. As shown, an optical delay line was used to retard the reference beam so that both beams could be detected with the same photomultiplier with a separation in time small compared to the characteristic drift times of the electronics. A charge integrating amplifier detected the signals and displayed them on the screen of an oscilloscope as a step function. The x-position of the first step served to record the interval following the e-beam discharge at which the afterglow was sampled. Time resolution was of the order of 6 nsec, but jitter of about 100 nsec rendered the measurement tedious. Long-term stability of the relative intensities between paths was of the order of 6% which determined minimal gain or loss which could be recorded with significance.

Figure 24 shows the topology of the map of gain resulting from measurement at 3 atmospheres pressure over the space of parameters indicated. Across the xz plane to the rear of the data has been plotted the time dependence of the spontaneous emission for scale. For comparison on the yz plane to the left edge is shown the normal emission spectrum of the $3s^3\Sigma_u^+ \rightarrow 2p^3\Pi_g$ transition, uncorrected for pressure and Stark broadening. As can be seen, the R-branch is absorptive while highest gains are found in the Q-branch head and P_4 and P_6

Figure 24

Fractional gain per round trip transit as a function of wavelength and time for the afterglow of a 3 atmosphere helium discharge as directly measured from the enhancement of a probing dye laser beam. Regions of stimulated emission lie above the x,y plane; absorption below. Across the x,z plane to the rear of the data has been plotted the time dependence of the spontaneous emission for scale and on the plane to the left edge is shown the normal emission spectrum of the $3s^3\Sigma_u^+ \rightarrow 2p^3\Pi_g$ transition of the He_2 uncorrected for broadening mechanisms.

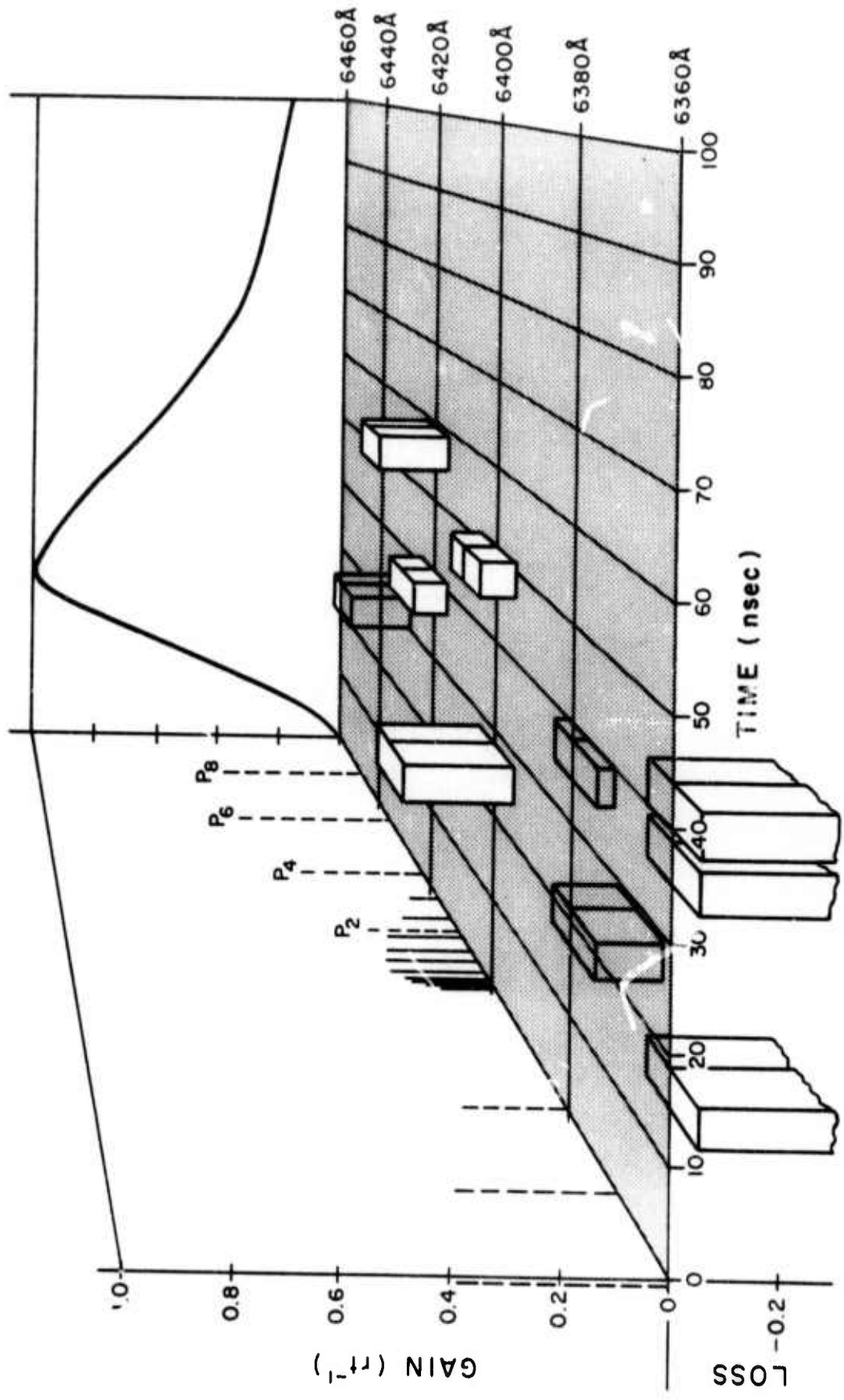
6460Å
6440Å
6420Å
6400Å
6380Å
6360Å
TIME (nsec)
GAIN (τ⁻¹)
LOSS
P8
P6
P4
P2

components. Higher members of the P-branch appear absorptive. Units plotted are the gain coefficient per round trip transit of the afterglow, so that the peak gain of 0.23 measured at the head of the Q-branch corresponds to a value of 0.04 cm^{-1} at 6400 Å.

Further confirmation of the magnitude of the gain was obtained from quantitative observations similar to those of the previous part d) of this section of the axial intensity emitted from a resonant cavity containing the plasma as a function of cavity length. Cavities were used in which the mean lifetime of a photon in the cavity considerably exceeded the lifetime of the amplifying medium. For these measurements, the dye laser was removed and a dielectric mirror of 99% reflectance at 6400 Å was added. Optics were used having solid angles of acceptance small compared to the solid angle spanned by the forward lobe of the radiation pattern from the cavity. Under these conditions, there is no geometric effect and the axial intensity is simply a function of the number of transits of the plasma a photon can make before the plasma decays and the gain or loss occurring during each transit.

If it is assumed that the small signal extinction coefficient, K, is proportional to the population of the excited states, then after n transits of the afterglow, it will be given approximately by

$$K = K_o \ell^{-\frac{2n\ell}{c\tau}} , \qquad (21)$$

where ℓ is the length of the resonant cavity and τ is the recombination lifetime. Considering discrete intervals of time equal to the duration of a complete round trip transit the energy, E, in the cavity resulting from the spontaneous emission during the first of these, will after n transits have been attenuated (or amplified) to

$$E(n) = I_o \frac{2\ell}{c} e^{-2K_o \ell \frac{c\tau}{2\ell}\left(1-e^{-\frac{2n\ell}{c\tau}}\right) - nL} \qquad (22)$$

where I_o is the initial spontaneous intensity and L is the passive cavity loss per round trip. During the n^{th} pass, the energy emitted axially from the cavity is approximately, $L \cdot E(n)$, assuming losses are primarily due to transmission. Then integrating over all transits, the energy emitted from the cavity as a result of the first increment of spontaneous emission $I_o(2\ell/C)$ is

$$E = \int_o^{\infty} \frac{\tau}{Q} \; LI_o e^{-2K_o \ell Q(1-e^{-n/Q})-nL} \; dn \quad , \qquad (23)$$

where now the parameters have been collected in terms of Q, the probable number of photon transits in a recombination lifetime, and

$$Q = \frac{c\tau}{2\ell} \quad . \qquad (24)$$

Through transformation of variables, this becomes

$$E = I_o \tau L e^{-\alpha} \int_o^1 z^{(QL-1)} \, e^{\alpha z} dz, \quad , \qquad (25)$$

where $\alpha = 2K_o \ell Q$ the mean fractional intensity decrease, and this is

$$E = I_o \tau L e^{-\alpha} (QL)^{-1} M(QL, QL+1, \alpha) \qquad (26)$$

where M is the confluent hypergeometric function.

For gain $\alpha = |\alpha|$ so letting $\beta = -|\alpha|$ and recognizing for each time increment there is an additional emission of spontaneous energy, then the substitutions.

$$I_o \rightarrow I_o e^{-p/Q} \qquad (27a)$$

$$K_o \rightarrow K_o e^{-p/Q} \qquad (27b)$$

must be made in (26). The resulting total energy emitted axially per pulse then becomes

$$\varepsilon = \int_0^\infty E dp = I_o \tau / Q \int e^{\beta_o} e^{-p/Q} e^{-p/Q} M(QL,\ QL+1, -\beta e^{-p/Q})\ dp \qquad (28)$$

Transforming variables, this becomes

$$\varepsilon = I_o \tau \beta_o^{-1} \int_0^{\beta_o} M(1, QL+1, x) dx \qquad . \qquad (29)$$

Expanding in terms of the usual infinite series for M(a,b,z) and factoring terms having useful limiting properties gives

$$\varepsilon = \varepsilon_o F(\beta_o, LQ) \qquad (30)$$

where

$$\varepsilon_o = I_o \tau (\beta_o)^{-1} \ (e^{\beta_o} - 1) \qquad , \qquad (31)$$

represents an emitted energy, characteristic of a simplified equivalent plasma of constant spontaneous intensity I_o, and gain per round trip (β_o/Q), (both decreasing discontinuously to zero after a lifetime τ) and a lossless cavity of length allowing Q complete transits during τ, and the corrective multiplicative correction function F is given by

$$F(\beta_o, LQ) = (e^{\beta_o} - 1)^{-1} \left\{ \beta_o + \sum_{m=1}^{\infty} \frac{1}{m+1} \frac{(\beta_o)^{m+1}}{(LQ+1)\ldots(LQ+m)} \right\} \qquad ; \qquad (32)$$

where F is of order unity for small gains and losses.

Data suitable for the evaluation of eq. (30) is shown in Figure 25. In this figure are shown the intensity emitted axially at 6400 Å from the cavity together with the spontaneous emission.

Figure 26 shows a plot of the axial intensity from which the passive

Figure 25

Time resolved enhancements of the intensity at 6400 Å observed in the resonant cavity during single e-beam excitations at three atmospheres of helium. In each photograph the uppermost curve is the enhanced intensity, the center curve is the normal afterglow emission, and the lower curve the background noise. Two different cavity lengths are shown at 46 cm and 29 cm. The horizontal time scale is 40 nanoseconds/division in each case.

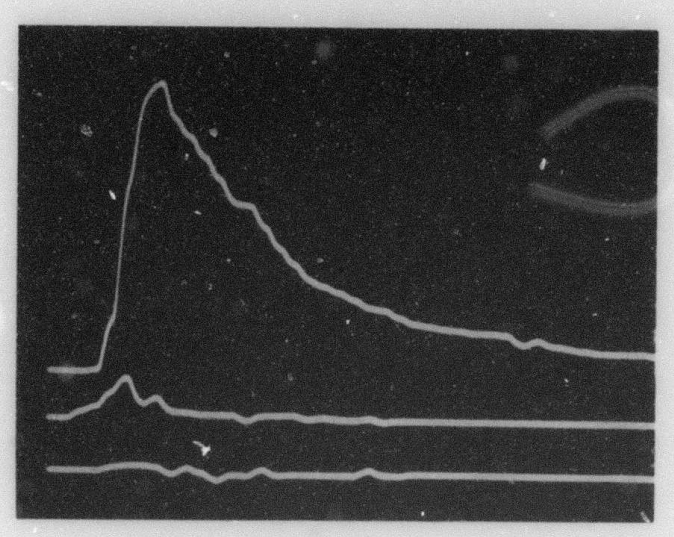

CAVITY
LENGTH
46 cm
RATIO
21:1

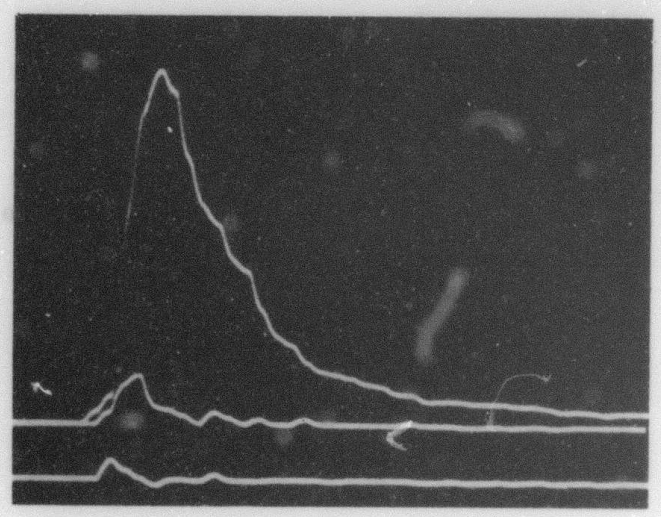

CAVITY
LENGTH
29 cm
RATIO
60:1

Figure 26

Logarithmic plot as a function of time of the intensity emitted axially at 6400 Å for a cavity of 53·3 cm. length. The straight line slope corresponding to a passive loss of 3.0% per round trip is shown.

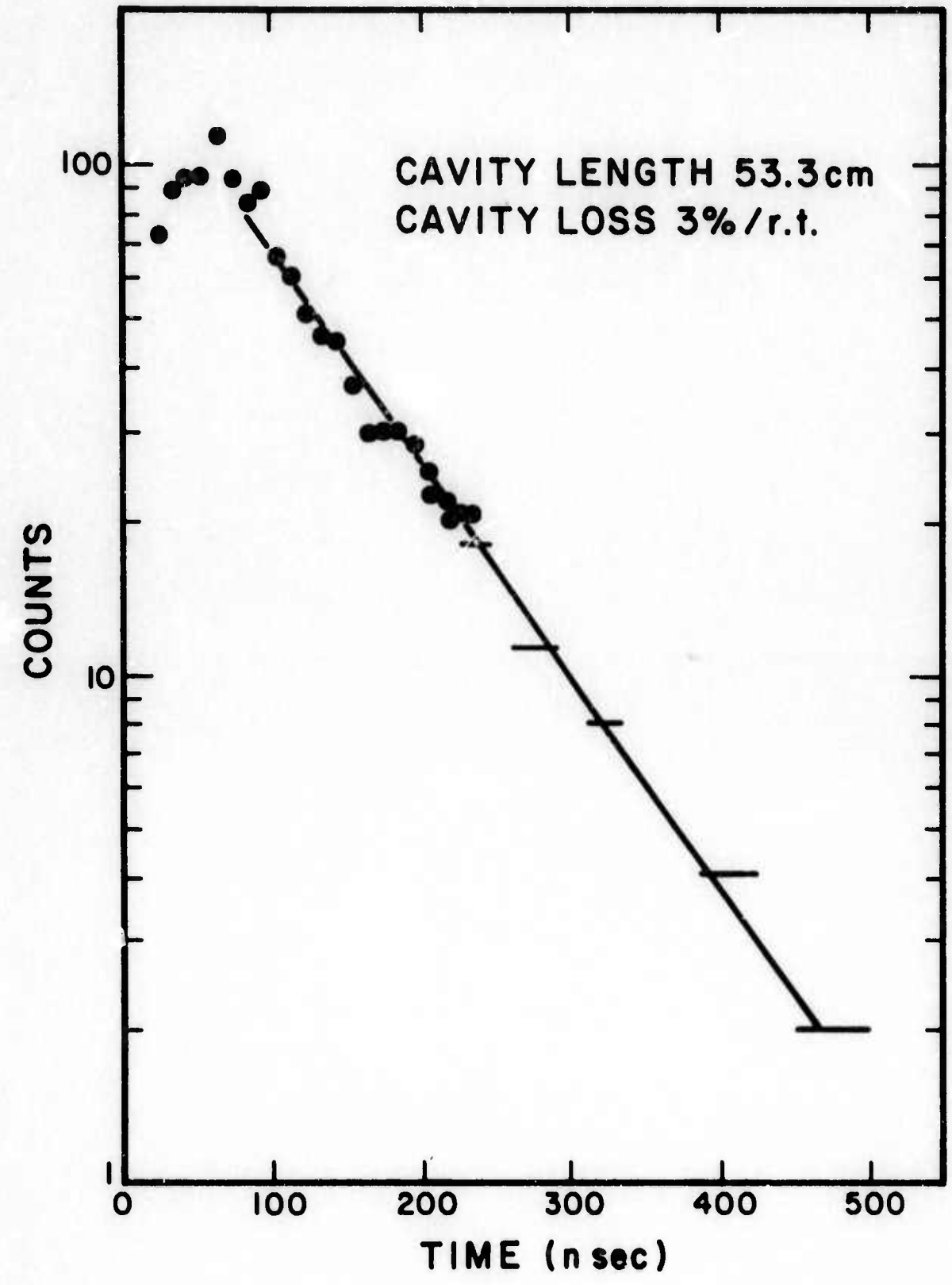
CAVITY LENGTH 53.3cm
CAVITY LOSS 3%/r.t.
COUNTS
100
10
1
0
100
200
300
400
500
TIME (n sec)

cavity loss can be determined. Correlation for various cavity lengths of the exponential decay times for the loss of intensity from the cavity following termination of the discharge afterglow gave a passive cavity loss of 3% per round trip. With this calibration equations (30) through (32) can be evaluated.

Figure 27 summarizes the resulting energy per pulse emitted axially at 6400 Å and normalized to the isotropic incoherent emission from the afterglow for cavities of four different lengths. Shown for comparison are curves modeling the expected growth of pulsed energy from the particular cavity according to (30) when containing an amplifying medium of 0.104, 0.124 and 0.144 $(\text{round trip})^{-1}$ peak gain and corrected according to (32) for a time-dependence of the gain proportional to that observed for the spontaneous emission. The best value at this pressure of 3 atmospheres appears to be 0.124 and corresponds to an average over the 45 Å FWHM bandpass of the 6413 Å interference filter used in the measurement. Comparison with Figure 24 identifies this as the average gain over the Q-branch and lower P-components and provides the agreement with the higher peak values resolved for certain of those components.

It appears the close correlation between the different measurement approaches confirms the existance of significant gain in the He_2 system. Research in progress now is expected to refine the data of Figure 24 and extend this type of direct measurement to the other bands of He_2 at 5130 Å and 4400 Å for other values of pressure.

f) Stimulated Output Efficiencies--The measurements of the previous part e) serve to give the first rough estimates of the efficiency of the stimulated emission observed. At the present time, characterization of the dye laser is incomplete, but the importance of even crude approximations to the output efficiency warrants

Figure 27

Functional dependence on the number of round-trip transits of the cavity made by a photon during the lifetime, τ, of the plasma, of the energy emitted axially per pulse from a resonant cavity enclosing the plasma and normalized to the energy of the spontaneous incoherent radiation. Wavelength was selected by an interference filter centered at 6413 Å with a FWHM of 45 Å and passive cavity losses were 0.03 per round trip. X - experimental date; solid curves--theoretical models given by equations(31) and(32) for values of fractional gain per round trip of 0.104, 0.124, and 0.144 as marked.

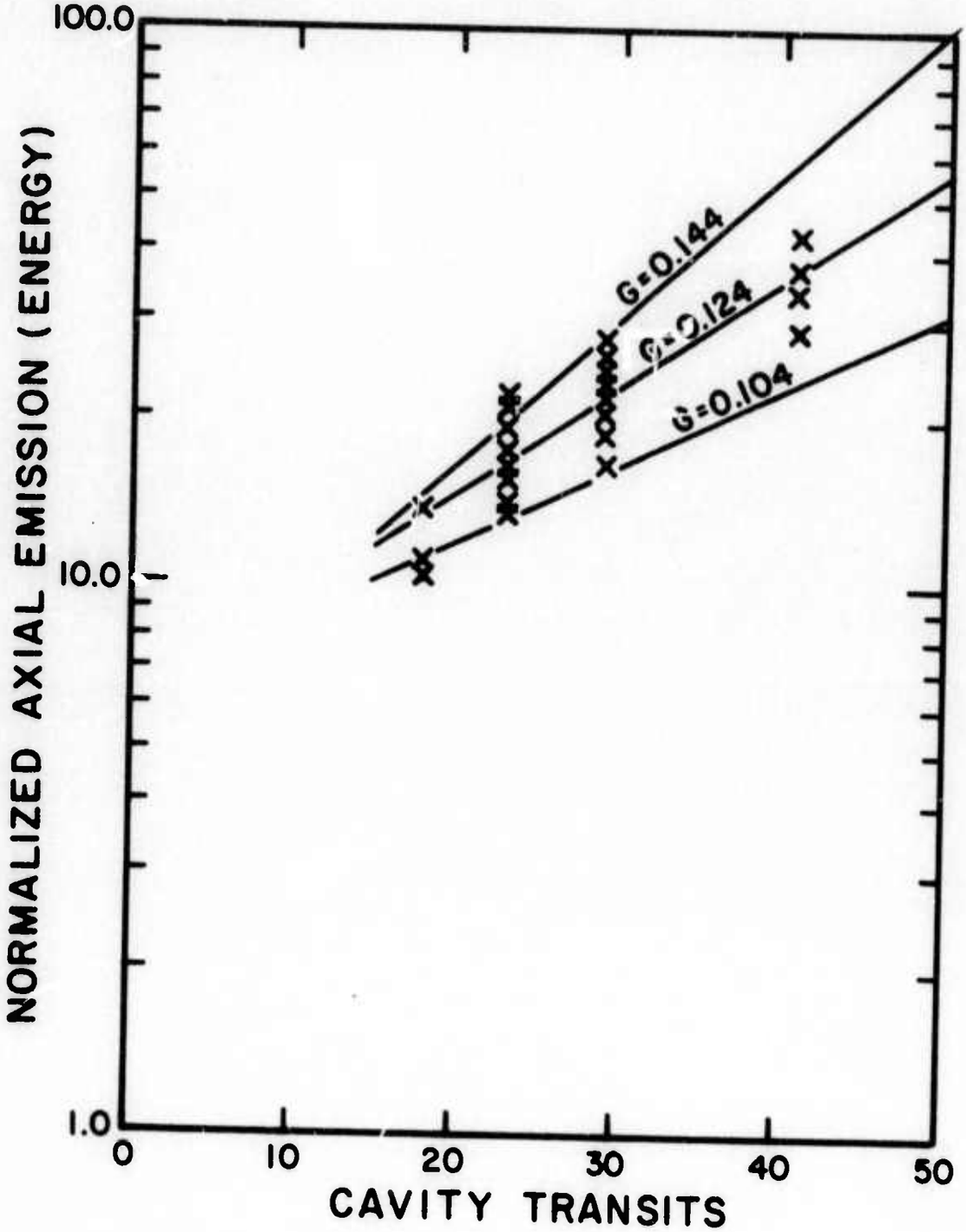
100.0
10.0
1.0
NORMALIZED AXIAL EMISSION (ENERGY)
G=0.144
G=0.124
G=0.104
0
10
20
30
40
50
CAVITY TRANSITS

their tentative use. Measurements with a ballistic thermopile have fixed the N_2 -laser pump energy at 1.5 mJ per pulse. Assuming a 20% conversion efficiency in the dye and 50% loss in the beam splitter, the probing energy at 6400 Å should be of the order of 0.15 mJ per pulse. Using the peak fractional gain of 0.23 from Figure 24 gives an energy for the stimulated emission of .035 mJ per pulse. Since the geometry of the beam was arranged to illuminate of the order of 1 cm^3 of afterglow, the energy extracted in the stimulated emission corresponded to a value of

$$E = 35 \text{ mJ/liter} \quad . \tag{33}$$

This was extracted from the afterglow in around 6 nsec so that the extracted power reached

$$P = 5MW/\text{liter} \tag{34}$$

with no evidence of saturation of the transition. In comparison with the 52.5$_\mu$ J/liter radiated spontaneously at 6400 Å, the value of (33) clearly indicates that the energy normally lost during the recombination to non-radiative channels of stabilization can be returned to an induced channel as stimulated emission.

From Table VI it can be seen the increased energy of stimulated emission raises those efficiencies to

$$\varepsilon(6400 \text{ Å}) \geq 0.6\% \tag{35}$$

for the overall efficiency of stimulated emission at 6400 Å. As there is no evidence saturation is occurring, it can be expected that a reduction in the cross-section of the probing beam will raise efficiencies close to the theoretical values of Table I. The implications of these results are discussed in the following section.

V. IMPLICATIONS

The most evident implication of the technical results presented in the previous section is that since stimulated emission has been observed with a significant extraction of energy, the feasibility of a recombination laser has been demonstrated. Had a longer gain-path length been available for the duration of the afterglow lifetime, a laser would have been realized. The more subtle implications are perhaps even more important. In particular:

(1) The results summarized in Table IV suggest that in helium collisional recombination does in fact offer a mechanism for optically recovering the majority of the excitation energy lost to ionization and wasted in analogous N_2 and H_2 e-beam laser systems.

(2) The relatively short lifetimes summarized for the He_2 system in Table III indicate that these are in fact recombination lifetimes, and the possibility of unrealized higher order terms slowing the recombination has not yet become a problem at 7 atmospheres. This is of considerable significance, as is indicated in Figure 7, because now the range of parameters spanned by extrapolations to the objective lifetime of a nanosecond is small compared to the range over which measurements are available.

Neither the reheating of the electrons by the stabilizing processes nor an unexpected saturation of the sequence has become a problem. As can be seen, the experimental points on the 1 to 7 atmosphere interval are consistent with theoretical calculations at an electron temperature of $1000^{o}K$. This temperature is in turn consistent with the extrapolations of the thermal economy calculations[13,14] which predict the degree of temperature rise produced by the superelastic stabilizing collisions.

Clearly there is a much stronger basis for extrapolating the results of both experiments at 0.1 atmosphere and 3.0 atmospheres to a lifetime of a few nanoseconds at 20 atmospheres than there was initially on the basis of the first measurement alone. In fact, the recombination rate coefficient corresponding to the 75 nanosecond lifetime and electron density

$$[e] = 5 \times 10^{14} \text{ cm}^{-3} \tag{36}$$

is

$$\alpha = 2.7 \times 10^{-8} \text{ cm}^3 \text{ sec}^{-1}$$

and represents one of the largest values measured for collisional recombination in the absence of dissociative recombination. It is confirming evidence that the parametric forms such as (4) can indeed be considered valid to such large values.

(3) The implication of the rather low efficiencies for the incoherent emission of radiation from the recombination as shown in Table VI is that much of the stabilization is carried by non-radiative collisional channels. However, in this case, the prospect for reducing the importance of such channels by the competition from a lasing channel is good in view of the high preliminary values of gain and the much higher efficiency, 0.6%, for the extraction of stimulated emission. Figure 28 presents the comparison of experiment and theory as a guide to potential extrapolation of energy available in the 6400 Å band. In the present experiment spontaneous emission is about three orders of magnitude below the energy corresponding to the quantum efficiency of the transition. The improvement introduced by stimulating the transition is seen to be substantial and in the rough approximations of Section IV e) appear to bring the energy extracted to within 20% of that theoretically

Figure 28

Energy/liter per pulse as a function of gas pressure calculated to be available to the 6400 Å transition in He_2 in the afterglow of the recombining e-beam discharge. The experimental points reported in this paper for spontaneous emission are shown by the open circles. The plus mark records the comparable value for the stimulated emission.

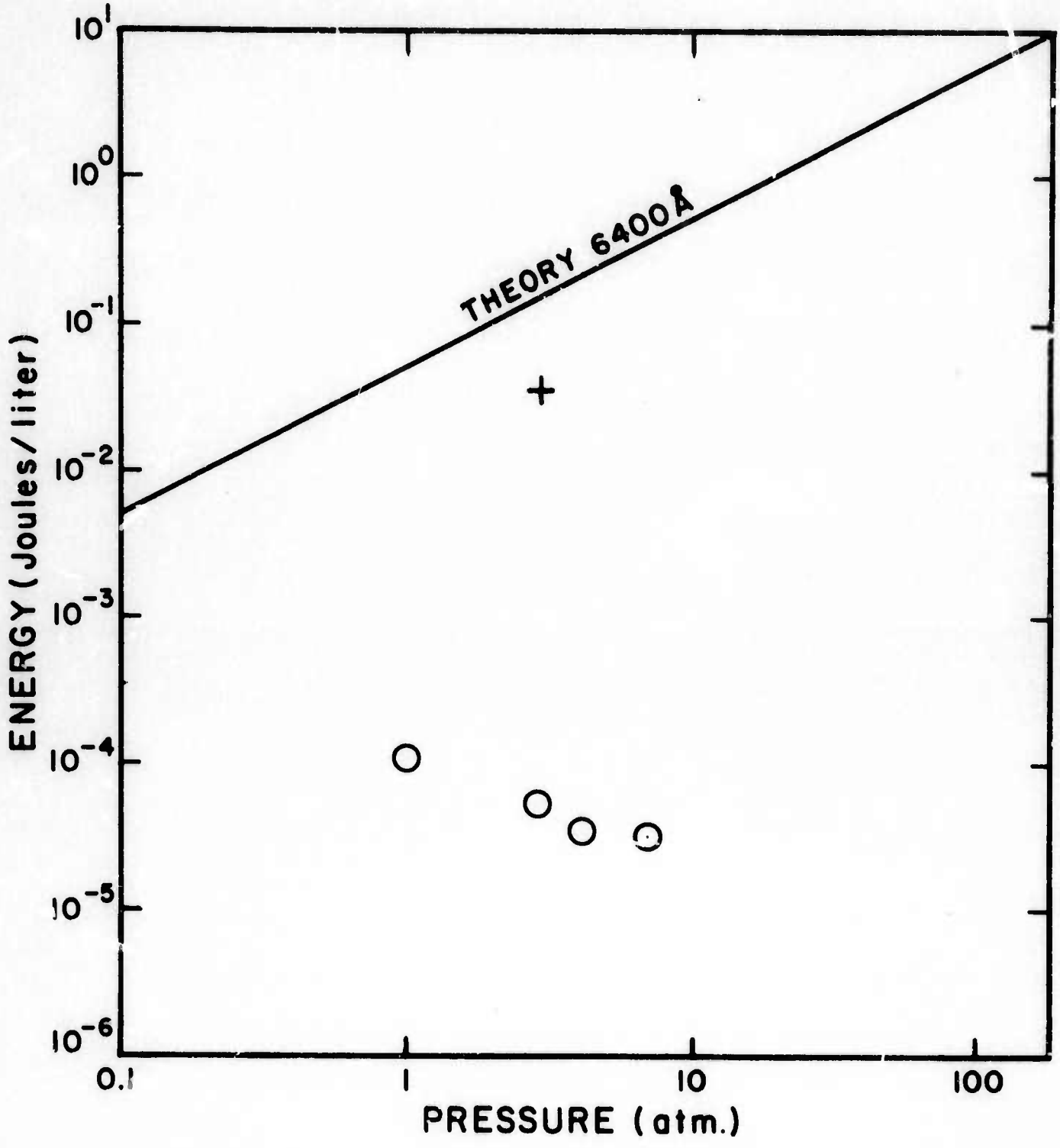
THEORY 6400Å
ENERGY (Joules/liter)
PRESSURE (atm.)
10^{1}
10^{0}
10^{-1}
10^{-2}
10^{-3}
10^{-4}
10^{-5}
10^{-6}
0.1
1
10
100

available. The further confirmation of these indications carries the highest priority as does their extension to shorter wavelength regions.

In summary it appears that the stimulated emission observed in this work confirms the importance of the collisionally stabilized mechanism as a source of population inversion of significance to the development of new types of high energy lasers depending upon electron beam excitation at high gas densities.

REFERENCES

1. C. B. Collins, Recombination Laser, Report No. UTDP A002-1, ONR Contract No. N00014-67-A-0310-0007, 1972.

2. C. B. Collins, A. J. Cunningham and B. W. Johnson, Recombination Laser, Report No. UTDP A003-1, ONR Contract No. N00014-67-A-0310-0007, 1973.

3. D. R. Bates, A. E. Kingston, and R. W. P. McWhirter, Proc. Roy. Soc. (London) A267, 297 (1962).

4. D. R. Bates and S. P. Khare, Proc. Phys. Soc. (London) 85, 231 (1965).

5. C. B. Collins, Phys. Rev. 177, 254 (1969).

6. C. B. Collins, Phys. Rev. 186, 113 (1969).

7. D. R. Bates and A. E. Kingston, Planet. Space Sci. 11, 1 (1963).

8. C.B. Collins, unplublished report.

9. J. Berlande, M. Cheret, R. Deloche, A. Gonfalone, and C. Manus, Phys. Rev. A1, 887 (1970).

10. E. Hinnov and J. G. Hirschberg, Phys. Rev. 125, 795 (1962).

11. C. B. Collins, H. S. Hicks, W. E. Wells, and R. Burton, Phys. Rev. 6, 1545 (1972).

12. C. B. Collins, H. S. Hicks, and W. E. Wells, Phys. Rev. A2, 797 (1970).

13. D. R. Bares and A. E. Kingston, Proc. Roy. Soc. A279, 10 (1964).

14. D. R. Bates and A. E. Kingston, Proc. Roy. Soc. A279, 32 (1964).

15. A. J. Cunningham, B. W. Johnson, and C. B. Collins, Phys. Lett (pending)

16. L.Blanaru, J. Appl. Phys. 44, 2735 (1973).

17. R. Ladenburg and F. Reiche, Ann. Physik, 42, 181 (1913).

APPENDIX I.

AFTERGLOW OF AN E-BEAM DISCHARGE IN SEVERAL ATMOSPHERES OF HELIUM*

A. J. Cunningham, B. W. Johnson, and C. B. Collins
The University of Texas at Dallas,
Dallas, Texas 75230

* This research was supported by the U. S. Advanced Research Projects Agency of the Department of Defense and monitored by ONR under Contract No. N00014-67-A-0310-0007.

ABSTRACT

Spectral observations of recombining helium afterglows at neutral pressures in the range 1 to 7 atmospheres and initial electron densities of $5 \times 10^{14} cm^{-3}$ are presented. Effective lifetimes against recombination of the principal atomic and molecular features are determined.

Because of the possibility[1] of obtaining population inversion as a consequence of the collisional-radiative recombination of hydrogenic ions with electrons, a considerable importance is attached to the basic study of this recombination process in very dense, high pressure afterglows. This paper reports the preliminary characterization of the spectra emitted from a recombining helium afterglow at neutral pressures in the one to seven atmosphere range with an initial electron density of $5 \times 10^{14} cm^{-3}$. In contrast to previous studies at these high densities[2,3] the work reported here provides the first direct observations of radiation emitted from a dense helium afterglow which is consistent with a recombination origin.

A Febetron 706 electron beam gun projecting single pulses of 500 KeV energy, 8KAmp. peak current and 3 nanosecond duration through a circular titanium foil window, of 0.001 inch thickness, welded to one end face of a rectangular (3"x3"x2") stainless steel cell was used to create the primary ionization in the high pressure test gas. The experimental cell, which could be evacuated to a pressure of 10^{-11} Torr and baked to 400°C was of standard UHV grade construction and was fitted with quartz windows on opposite side faces to allow spectroscopic observations to be conducted on a lamina of plasma, transverse to the e-beam, which was excited by primary electrons of equivalent distance from the plane of entry into the test gas.

Spectra obtained using a spectrograph-image intensifier combination are shown in Figure 1 with the principal features identified. Peak

incoherent energy occured at 5875A° and peak incoherent power was observed at 6400A°. An f/4 spectrograph together with a nine stage photomultiplier, of 1.5 nanosecond risetime, and useable range of sensitivity from 3000 Å to 8500 Å, allowed the transient intensity dependence for particular 100 Å wavelength regions of the spectrum to be monitored with nanosecond resolution. Each of the spectral features in the wavelength range of the instrumentation showed either one or a combination of three basic transient responses, each correlating with a different excitation mechanism. These are illustrated and summarized as nearly as possible in Figure 2. In the case of the molecular light all decay times were equivalent to within experimental precision while each atomic line had its characteristic time constant for decay varying from the common molecular value to much longer times.

Quantitive comparison of the intensity decay times attributed to ion-electron recombination can be made by starting from the general parameterization[4] for the effective two-body recombination rate coefficient, α,

$$\alpha = K[e]^{\eta} (T_e/300)^{-9/2} \qquad (1)$$

where [e] denotes the free electron concentration, T_e the electron temperature and η is an exponent between 0.0 and 1.0 reflecting the two or three body character of the recombination respectively. This gives the intensity model

$$\frac{d}{dt}\left[I - \frac{1+\eta}{2+\eta}\right] = (1+\eta)\left[I_o - \frac{1+\eta}{2+\eta}\right]\tau^{-1} \qquad (2)$$

where I is the time-varying intensity decaying from some initial value I_o and $\tau^{-1} = \alpha [e]_o$ is the inverse of the effective lifetime against recombination at the initial time corresponding to I_o.

The effective lifetime against recombination can then be determined from inverse slope of the linear portion of a graph of the inverse intensity to a single power as a function of decay time as suggested by equation 2. Such a plot for the molecular band at 6400A° is shown in Figure 3 for η=1 and yields a τ value of 82×10^{-9} sec. at 3 atmospheres of helium. Lifetimes for the principal features observed are shown in Table 1. These results attest to the importance of the afterglow period to the radiative economy of such high density, electron beam discharges and confirm the significance of the recombination mechanism as a source of excited state population leading to the potential of much higher system efficiencies for high-energy gas lasers depending upon electron beam excitation at high gas densities.

Table I. Lifetimes (nanoseconds) Against Recombination of the Principal Spectral Features of the High Pressure Helium Afterglow.

Wavelength		Pressure (atm.) 1	3	4.2	7
6400 Å	He_2	160	82	59	26
4650 Å	He_2	130	82	53	34
7065 Å	He	-	267	350	93
6678 Å	He	208	100	45	29
5875 Å	He	Early 880	490	425	300
		Late 2800	3800	2700	2320

REFERENCES

1. C. B. Collins, A. J. Cunningham and B. W. Johnson, Abstracts 25th Gaseous Electronics Conference London, Ont. Canada. 153, Oct. 1972.

2. F. Robben and E. Hagberg, Aktiebolaget Atomenergi, Stockholm, Report No TDM-FFA-762, 1967 (unpublished).

3. M. Bourène and J. LeCalvé, J. de Phys. 32, 29 (1971)

4. C. B. Collins, H. S. Hicks, and W. E. Wells, Phys. Rev. A2, 797 (1970).

CAPTIONS

Figure 1: Survey spectrum of the visible region recorded with an f/4 spectrograph-image intensifier combination. Each spectrum is a time integrated record of the afterglow from a single discharge of the e-beam gun in helium at three atmospheres pressure. Two exposures at different image intensifier accelerating voltages of 30 and 35 KV are shown.

Figure 2: Time evolution of selected atomic and molecular emissions illustrating the three basic excitation mechanisms observed: 1) 5015 Å atomic transition, direct excitation by primary electrons 2) 7065 Å atomic transition, excitation by energetic secondary electrons and 3) 6400Å molecular transition, excitation via recombination of He_2^+ ions and cool secondary electrons.

Figure 3: Graph of Intensity to the inverse 0.66 power, (η=1 in equation 2) as a function of time during the afterglow period at a neutral gas pressure of three atmospheres.

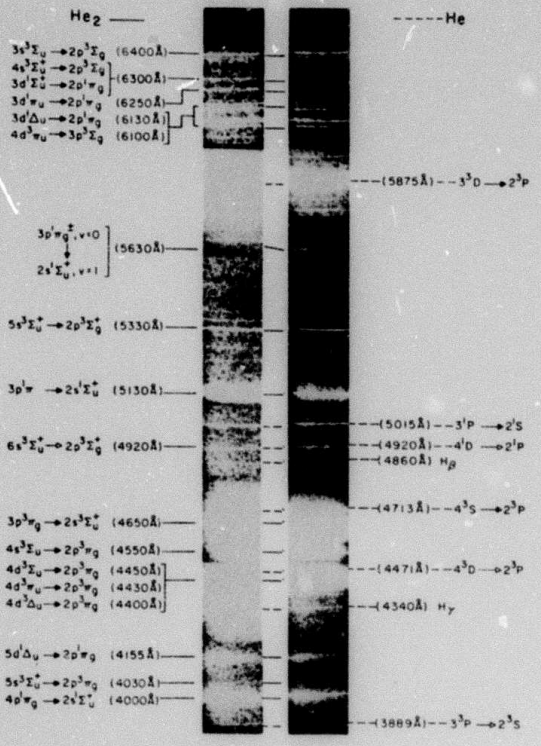
He2
He
3s³Σu → 2p³Σg (6400Å)
4s³Σu → 2p³Σg
3d¹Σu → 2p¹πg (6300Å)
3d¹πu → 2p¹πg (6250Å)
3d¹Δu → 2p¹πg (6130Å)
4d³πu → 3p³Σg (6100Å)
(5875Å) 3³D → 2³P
3p¹πg ±, v=0
2s¹Σu+, v=1 (5630Å)
5s³Σu+ → 2p³Σg+ (5330Å)
3p¹π → 2s¹Σu+ (5130Å)
(5015Å) 3¹P → 2¹S
6s³Σu+ → 2p³Σg+ (4920Å)
(4920Å) 4¹D → 2¹P
(4860Å) Hβ
3p³πg → 2s³Σu+ (4650Å)
(4713Å) 4³S → 2³P
4s³Σu → 2p³πg (4550Å)
4d³Σu → 2p³πg (4450Å)
4d³πu → 2p³πg (4430Å)
4d³Δu → 2p³πg (4400Å)
(4471Å) 4³D → 2³P
(4340Å) Hγ
5d¹Δu → 2p¹πg (4155Å)
5s³Σu+ → 2p³πg (4030Å)
4p¹πg → 2s¹Σu+ (4000Å)
(3889Å) 3³P → 2³S

III.

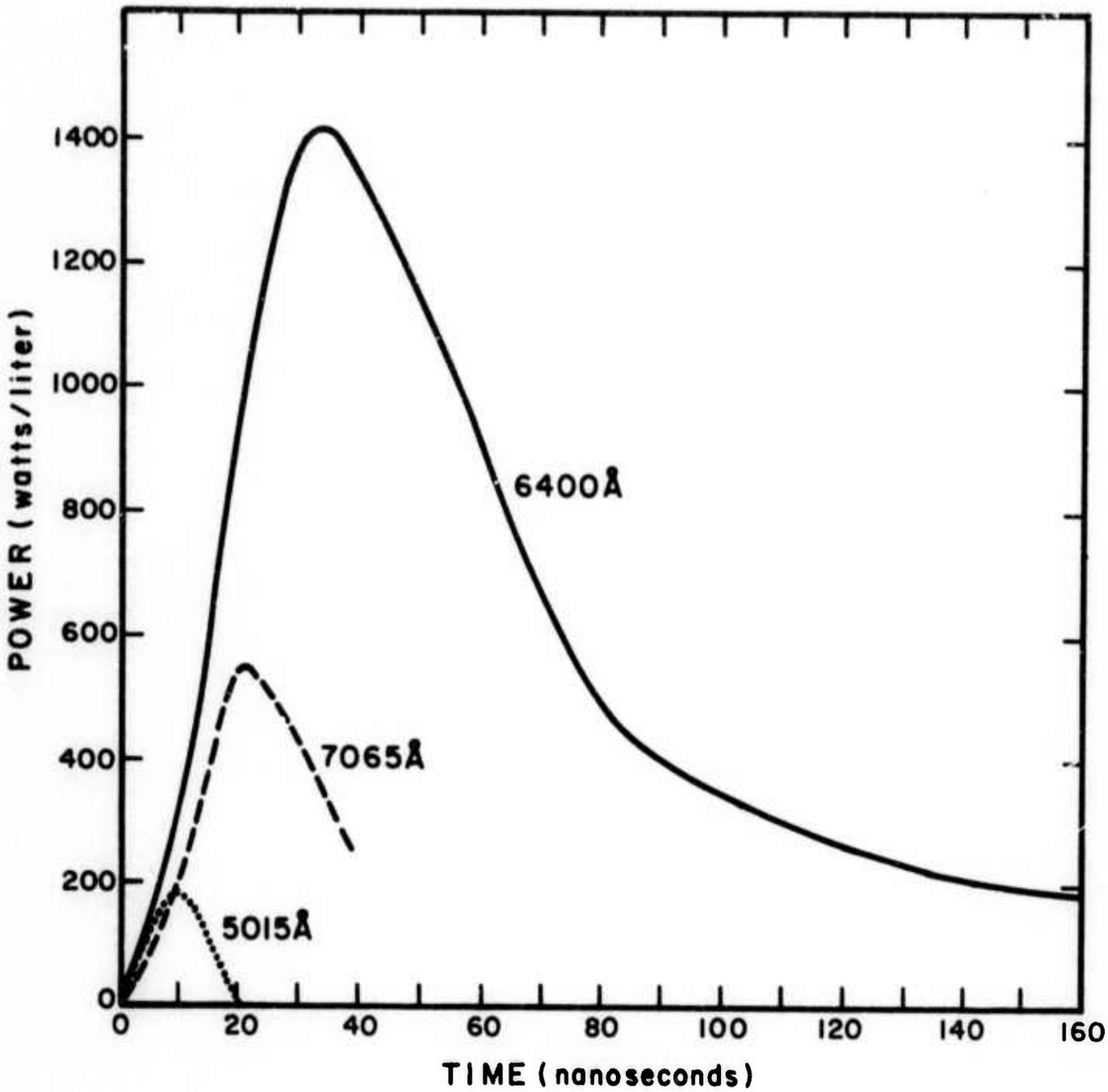
POWER (watts/liter)
1400
1200
1000
800
600
400
200
0
6400Å
7065Å
5015Å
0
20
40
60
80
100
120
140
160
TIME (nanoseconds)

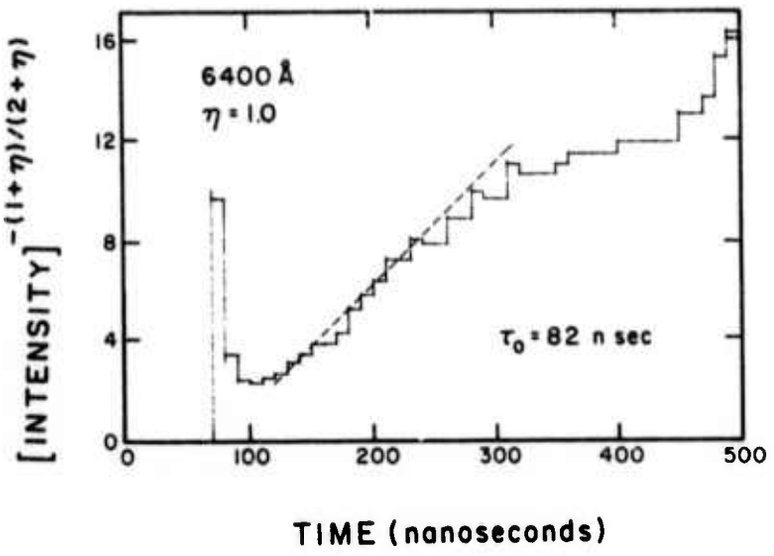
6400 Å
η = 1.0
τ0 = 82 n sec
[INTENSITY]^-(1+η)/(2+η)
TIME (nanoseconds)
0
4
8
12
16
0
100
200
300
400
500